AMERICAN UNIVERSITY OF BEIRUT

SELF-ASSEMBLY OF CHITOSAN OLIGOSACCHARIDE LACTATE AND ITS INTERACTION WITH CURCUMIN: EXTENSION TO AN ENZYME-FREE CHOLESTEROL SENSOR USING NANO-HYBRID STRUCTURE

by
MAZHAR MARWAN CHEBL

A thesis
submitted in partial fulfillment of the requirements
for the degree of Master of Science
to the Department of Chemistry
of the Faculty of Arts and Sciences
at the American University of Beirut

Beirut, Lebanon
July 2016

AMERICAN UNIVERSITY OF BEIRUT

SELF-ASSEMBLY OF CHITOSAN OLIGOSACCHARIDE LACTATE AND ITS INTERACTION WITH CURCUMIN: EXTENSION TO AN ENZYME-FREE CHOLESTEROL SENSOR USING NANO-HYBRID STRUCTURE

by

MAZHAR MARWAN CHEBL

Approved by:

Digambara Patra

Dr. Digambara Patra, Associate Professor — Advisor
Chemistry

Dr. Faraj Hasanayn, Professor — Member of Committee
Chemistry

Dr. Houssam El-Rassy, Associate Professor — Member of Committee
Chemistry

Date of thesis defense: July 01, 2016

AMERICAN UNIVERSITY OF BEIRUT

THESIS, DISSERTATION, PROJECT RELEASE FORM

Student Name: Chebl Mazhar Marwan
Last First Middle

☒ Master's Thesis ○ Master's Project ○ Doctoral Dissertation

☒ I authorize the American University of Beirut to: (a) reproduce hard or electronic copies of my thesis, dissertation, or project; (b) include such copies in the archives and digital repositories of the University; and (c) make freely available such copies to third parties for research or educational purposes.

☐ I authorize the American University of Beirut, **three years after the date of submitting my thesis, dissertation, or project,** to: (a) reproduce hard or electronic copies of it; (b) include such copies in the archives and digital repositories of the University; and (c) make freely available such copies to third parties for research or educational purposes.

Mazhar Chebl 19-07-2016
Signature Date

ACKNOWLEDGMENTS

First of all, I would like to thank my advisor and mentor Dr. Patra for his guidance and patience throughout my master degree. Thank you for every piece of advice you gave me. All the scientific knowledge and curiosity you passed to me will be of great importance to me in the coming years as a PhD student, and in life in general.

I would like to express my gratitude to the committee members Dr. Hasanayn and Dr. El-Rassy for the knowledge and experience that you shared with us, whether in class or in the laboratory. It was a pleasure being your student.

Special thanks to the CRSL members; Dr. Mneimneh, Juan, Rania, Chadi and Samer for their technical support and assistance.

Thank you to all the professors and doctors who were such a help and played such an important role in the past three years. Without you I wouldn't be writing this right now

I would also like to thank all of the graduate students for their support and backup in the last few years. Zeinab, Elsy, Riham, Razan, Anto, Maya, Tina, Sandrine, Ali Mougharbel and Simona. Thank you for putting up with me in the lab and for your patience and help. And to all the graduates, we went through the same ups and downs, and it was my pleasure being there with you.

Finally, I would like to thank my parents and family for their support. Thank you for believing in me and always pushing me forward.

AN ABSTRACT OF THE THESIS

Mazhar Marwan Chebl for Master of Science
Major: Chemistry

Title: Self-assembly of chitosan oligosaccharide lactate and its interaction with curcumin: Extension to an enzyme free cholesterol sensor using nano-hybrid structure

Chitosan, is water lowly soluble polysaccharide. It has a high amine function density along its chain. This characteristic makes it soluble in acidic media. In addition to other properties it is biodegradable and biocompatible that broadens its biological application. On the other hand, extensive research is currently being held on curcumin due to its therapeutic benefits, which remains limited due to its low bioavailability and poor stability. Therefore, several methods were developed for curcumin encapsulation and incorporation in different systems in order to improve its delivery. At the same time recently use of curcumin as a fluorescent probe is being realized as its fluorescence spectral properties are sensitive to environmental changes.

In this work, Chitosan Oligosaccharide Lactate (COL), which is a modified form of chitosan to improve water solubility of chitosan, especially for the uses in drug delivery and biomedical applications, is studied in solution. The self-assembly of COL in aqueous environment has been investigated. Fluorescence of curcumin has been followed to determine the concentration at which chitosan aggregates, known as *critical aggregation concentration* (*cac*) and compared with other conventionally adopted methods such as electrical conductivity and fluorescence of pyrene. The size has been estimated using Scanning Electron Microscopy (SEM). It is found that self-assembly of COL in solution forms nano-aggregates of size 10-30 nm with a *(cac)* of ~5 μM. Fluorescence quenching of pyrene establishes that one COL chain may form around 5 independent hydrophobic microdomains during self-assembly in solution that are crucial to drug-polymer contact. Binding constant of curcumin and its partition coefficient with COL have been determined in double distilled water and at different ionic strength. Interaction of COL curcumin implies two different kinds of binding mechanisms of curcumin with the pre- and nano-aggregated forms of COL; respectively. A strong ground state interaction between curcumin and nano-aggregated COL has been noted with an association constant of 3.91×10^4 liters/moles at 298 K. This association has been found to be diffusion controlled, enthalpy driven and as consequences of hydrophobic effects due to Van der Waal's interactions. Increase in ionic strength, such as NaCl concentration, in the medium pushes the hydrophobic chain of COL and curcumin out from the solution by marginally lowering the *cac* and increasing the size (~30-60 nm) of the nano-aggregate, thus, it also exponentially boosts the partition of curcumin into COL nano-aggregates. However, similar increase in NaCl

concentration in the medium discourages contact of curcumin with pre-aggregated COL confirming an electrostatic interaction between curcumin and pre-aggregated form of COL. This is further supported by FT-IR spectra. On the other hand, hydrophobic bile salt surges both the *cac* and size of nano-aggregates (~100 nm) indicating bulky and hydrophobic cholate/deoxycholate group cooperatively binds with COL and curcumin for which higher concentration of COL is needed to accommodate bulky size of cholate/deoxycholate and form large nano-aggregates.

Chitosan has a pKa value in the range 5.5 to 6.5 and COL in acidic solution (at pH 2.8) forms polyelectrolyte due to protonation of the amine group. The positively charged amine function along chitosan chain in acidic medium can bind to a negatively charged silica nanoparticle forming nano hybrid particles (NHPs). To enhance stability and partition of curcumin into COL, NHPs have been prepared by self-assembly method. The self-assembly of COL has achieved using silica nanoparticles (SiO_2 NPs). Applying a novel nano hybrid biomaterials we demonstrate that analytical specificity can be further improved for a representative targeted biomedical species such as cholesterol without using any enzymatic reaction. As a proof of concept, here it is established that curcumin integrated chitosan oligosaccharide lactate (COL) self-assembles on silica nanoparticle surface to form nano hybrid particles (NHPs) of size in the ranges 25 – 35 nm with silica nanoparticle as its core and curcumin-COL as outer layer having thickness of 4-8 nm. The fluorescence intensity of these NHPs are found to be quenched and emission maximum is ~50 nm red shifted compared to free curcumin implying inner filter effect and/or homo-FRET between curcumin molecules present on the surface of individual nano hybrid particle. Although fluorescence of free curcumin is remarkably quenched by Hg^{2+} and Cu^{2+} ions due to chelation through keto-enol form, the fluorescence of NHPs is unaffected by Hg^{2+} or Cu^{2+} ion that boosts analytical selectivity. The fluorescence intensity is exceptionally enhanced in the presence of cholesterol but is not influenced by ascorbic acid, uric acid, glucose, albumin, lipid and other potential interfering substances that obstruct during enzymatic reaction. The interaction between cholesterol and NHPs is found to be a combination of ground state electrostatic interaction through the free hydroxyl group of cholesterol along with hydrophobic interaction between NHPs and cholesterol and excited state interaction. NHPs also outstandingly improve analytical specificity, selectivity and sensitivity during cholesterol estimation compared to free curcumin. The proposed cholesterol biosensor illustrates a wider linear dynamic range, 0.002-10 mM, needed for biomedical application and better than reported values during enzymatic reaction. In addition, the NHPs are found to be photo-stable potentially making it suitable for simple, quick and cost-effective cholesterol estimation and opening an alternative approach other than enzymatic reaction using nano hybrid structure to tune analytical specificity, selectivity and sensitivity of probe molecule.

CONTENTS

ILLUSTRATIONS

TABLES

CHAPTER I

INTRODUCTION

A. Chitosan

Known as fungine, chitin was first identified and described by Henri Braconnot in 1810 from mushroom extract[1], to be later on reported in insects in 1821[2]. Whereas chitosan was synthetized in 1859 by the action of boiled potassium hydroxide solution on chitin[3], but has not gained its name as chitosan until 1894 by Hoppe-Seyler and its structure as a copolymer of N-acetyl-D-glucosamine and D-glucosamine to be revealed later years[4].

Nowadays, chitosan and chitin are differentiated by their degree of deacetylation and are produced mainly from shrimps and crabs which are considered as a renewable chitosan source.

1. Properties and structure

Chitin, a natural linear polymer, is made of N-acetyl-D-glucosamine unit. After chitin treatment, and when the degree of deacetylation reaches 50%, chitosan is obtained; which is a random distribution of D-glucosamine and N-acetyl-D-glucosamine units.

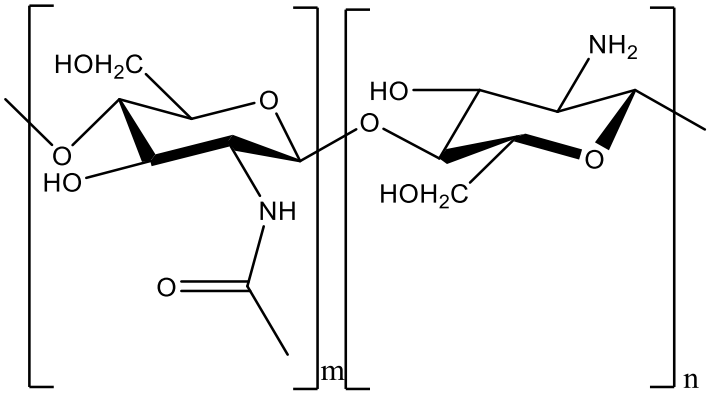

Figure I.1Chitosan/Chitin structure

Unlike chitosan, chitin is hydrophobic and insoluble in water. Chitin is extracted from living organisms (exoskeleton of arthropods, cell walls of fungi and yeast), acid treated to dissolve carbonate followed by alkaline extraction [5] and chitosan is obtained. The properties of chitosan depend on its origin, the structure, and the characteristics of the polymeric chain, which as well depends on the amount of NaOH used, extraction temperature and time; besides the previously mentioned chemical extraction, a relatively time consuming enzymatic extraction under mild conditions can be used.

The degree of acetylation is the ratio of acetylated groups over the total chain monomers, $DA = \frac{CH_3CO-}{-NH_2 + CH_3CO-}$ (1.1)

Titration, IR and UV-Vis spectroscopy are used to determine the degree of acetylation, but ^{1}H NMR remains the most common technique. As the degree of deacetylation increases the proportion of amine groups increases, therefore an increase in chitosan solubility.

The presence of the amine group obtained by chitin deacetylation gives chitosan a slightly basic aspect ($pK_a \approx 6.3$) and thus, it gets protonated in diluted acidic medium such as in HCl, 1% acetic acid, formic and lactic acid; but not soluble in sulfuric or phosphoric acid[6-8].

2. Application

In addition to the presence of the primary and secondary hydroxyl group, the amine moiety provided chitosan a broad range of modification reaction in order to improve its physical and biological properties.

The biocompatibility, biodegradability and low toxicity of chitosan[9] makes it an emergent material serving various application.

a. Biochemical and biological application:

Chitosan can be used as a scaffold material in tissue engineering [10, 11],providing cells with vital nutriments and adequate for cell adhesion and proliferation. Moreover, chitosan impregnated bandages are FDA approved in case of emergency [12].

Chitosan based material exhibits antibacterial [13], and antitumoric activity [14-16], and act as a food preservative taking advantages of its antioxidant properties [17].

Different routes for the synthesis of a chitosan based nanostructure have been adapted (emulsion cross linking, precipitation, ionotropic gelation…) and extensively used in delivery system [18]:

- In gene delivery: the presence of the positively charged amine function in acidic medium helps with the complexation to the phosphate group of the nucleic acid forming a polyplex, the entrapment of the nucleic acid can be enhanced by the addition of crosslinking agent such alginate. Also the degree of deacetylation and chitosan molecular weight affect the binging efficiency.
- In drug delivery: chitosan nanoparticles boost the trans-mucosal permeability and improve the para-cellular transport; these characteristics made of them a drug carrier for controlled release helps overcome the lack of solubility of hydrophobic drugs, thus enhancing their bioavailability and bio-distribution.
- Protein, and peptide delivery : Pan et al.[19] have reported insulin oral administration using chitosan nanoparticles. This system has shown an improvement in lowering plasma glucose level due to the protective mechanism of the nanoparticles and the chitosan ability to enhance insulin absorption through the intestine epithelial cells.

b. Application in Chemistry:

The high nitrogen percent in chitosan made of it an excellent chelating agent for metal. Singhon el al [20] have reported the use of silica chitosan composite for Ni^{2+} adsorption at pH 5 and 7.

Others have used chitosan and chitosan derivatives for Hg^{2+}, Cu^{2+}, and Pb^{2+} [21, 22] where a moderate pH (5-7) has been to be best for metal adsorption, whereas in the case of metal-anion adsorption [23] an acidic pH around 3 is required for the adsorption in order to protonate the amine function and hence improve the adsorption capability.

Chitosan hydro-beads, have been also used to for dye removal. Methylene blue, a cationic dye, shows an increased affinity toward chitosan beads at higher pH [24]; whereas the adsorption of congo red, an anionic dye, decrease as the pH increases [25].

Huang el al [26] have studied the formation of silver, gold, platinum and palladium chitosan nanocomposite. Zinc oxide –chitosan composite and graphene-chitosan electrode have been also prepared, where chitosan served for enzyme immobilization for cholesterol and glucose bio-sensing [27-37].

3. Chitosan modification

The abundancy of the amine and hydroxyl groups along the chain, makes chitosan an easy polymer to derive from. Among the modification that can chitosan undergoes, gel formation has gained a huge interest in drug delivery, swelling capability and adsorption studies.

In their review paper [38], Giri et al, summarized various modification leading to hydrogel formation which are :

- Covalent crosslinking: by the action of –C=O of the cross-linker; glutaraldehyde and oxalic acid are among the widely used crosslinking agents forming imine bonds with chitosan amino group.
- Ionic crosslinking: the positively charged amine groups of chitosan in acidic medium, can react with a negatively charged electrolytes forming ionic bridges. Among the anionic cross-linkers we cite: polyphosphate and Mo (VI) polyoxyanions [39].
- Grafting techniques: several initiators (free radicals, radiation and enzymes) were used to graft a monomer on the functional groups of chitosan. The

properties of the modified chitosan depends on grafting percentage influenced by monomer and initiator concentration and medium temperature [40].

These modified chitosan material, form a hydrogel that are known for their capability of swelling large amount of distilled water at equilibrium, that decreases as the ionic strength of the medium increases [39]. On the other hand, X. Qu et al [41] have reported that swelling of lactic acid and glycolic acid- chitosan hydrogel to be pH dependent: a better swelling ability has been observed in acidic medium where $–NH_2$ are ionized, increasing by this the pores volume as a result of electrostatic repulsion of the amine groups.

Moreover, chitosan has been incorporated in several matrixes and material (ɣ-Fe_2O_3, magnetite, sand…) to improve their properties. Several chitosan composite materials have been developed for waste water treatment. Another kind of chitosan modification by crosslinking with silica, forming a hybrid mesoporous material by a sol-gel process and studied for similar application as discussed above.

B. Micelle

Micellization, is a process by which individual molecules self-assemble to form a certain structure called micelle, an aggregation of molecules governed by hydrophobic interaction between chains.

A standard micelle model is formed by amphiphilic molecules made of a polar head in contact with water molecules and a long hydrophobic alkyl chain forming the core of the micelle.

It's well known that monomers can't form micelle unless their concentration is above a certain limit, the critical micelle concentration (CMC), below which the physico-chemical properties of the solution differ than that at concentration above the CMC. Tracking these changes versus monomer concentration help in CMC determination. Among the techniques used, common methods are by measuring properties like conductivity, surface tension, dye fluorescence, refractive index, viscosity, etc.

The factors that affect the CMC value of a given surfactant are [42]:

- Hydrocarbon chain length: an increase in the carbon atoms number (n_c) of the alkyl chain lead to a decrease of the CMC because of the increase in the hydrophobic effect This change is expressed by the following expression: $log(CMC) = a - bn_c$ where a and b are constants.
- The presence of unsaturation in the alkyl chain lead to an increase in the CMC value compared to a saturated hydrocarbon chain.
- Polar substitution in the alkyl chain is expressed by an increase in the surfactant solubility and thus higher CMC value.
- The presence of polyelectrolyte in solution lower the CMC of an ionic surfactant, but its effect is negligible for nonionic surfactant.

C. Curcumin

Curcumin also known as (1E, 6E)-1, 7(4-hydroxy-3-methoxyphenyl)-1, 6 heptadiene-3,5dione, is the principal compound of curcuminoid extracted from turmeric.

Traditionally, curcumin is an important ingredient in Asian cuisine as a food colorant and food additive to spice up curry, salads and sauces.

Besides being used in dietary application, curcumin was and still being applied in medicinal and therapeutic aims as an antioxidant, antitumeric and for Alzheimer treatment due to its biocompatible and biodegradable properties. Moreover curcumin have found application as a sensing probe [43, 44], and a reducing agent [45].

1. Photo physical properties:

Curcumin, is a yellow-orange powder of a molecular mass 368.38 g/mol and is soluble in organic solvent but poorly soluble in water. Its absorption maximum is around 408-430 nm and emits in the range 540-600 nm depending on the solvent used [46] and it has a relatively low quantum yield as well as a short life time[47].

Curcumin exists under as a β-diketone form as well as enol form as below:

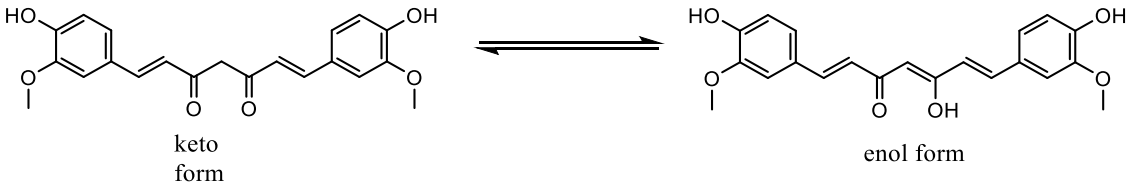

Figure I.2 Curcumin tautomerization

The proportion of enol to keto form depends on the temperature and the properties of the solvent. X-ray diffraction pattern and DFT studies suggest the stability of cis-enol form in vacuum and solution due to the conjugation of the π-electron system and the enolisable hydrogen is evenly distributed between the two oxygens. However, NMR studies show that curcumin exists as an enolic isomer in non-polar and aprotic solvents, whereas in protic solvents, the intramolecular hydrogen bonding is ruptured favoring the formation of the keto form[48].

The broad absorption band in the range of 410-300 nm is due to the π- π* transition and theoretical studies predict the absorption maxima at 389 and 419 nm for the keto form and enol form respectively. The presence of a donor o-methoxy phenyl and an acceptor –C=O group in curcumin lead to an increase of 6.1D[46] in the dipole moment of the first excited state from that of the ground state meaning that the excited state is more polar than the ground state.

DFT studies show that the dihedral angel of the enol form is 180° whereas it's twisted in the keto form with a torsion angel of 74°[49] .

Concerning curcumin stability, Wang et al. [50] have studied curcumin degradation in buffer solution, where in acidic medium is more stable than in basic medium due to the conjugated diene structure. Moreover, curcumin photo-degradation has been reported and resulted in vanillin and p-hydroxybenzaldehyde as a by-products[51].

2. Applications in biochemistry

The low bioavailability, and solubility of lipophilic molecules such as curcumin have initiated several attempts to incorporate and embed curcumin in different matrix in order to overcome these problems [52, 53]. Moreover, curcumin loaded biocompatible systems (liposomes, cellulose, biopolymer...) have shown an improved antitumeric activity [54-56],a photo induced anticancer effect and cell imaging [57, 58] and incorporated into various drug carrier systems for infections treatment due its antimicrobial activity[59].

Nevertheless, the presence of two phenolic groups of curcumin provide scavenging properties of ROS leading to the formation of a phenoxyl radicals which are less reactive than the peroxyl radicals [60].

3. Application in chemistry

The broad absorbance spectrum of curcumin (350-500 nm) in the near UV-Visible range offered curcumin the capability to be used as a photosensitizer in dyes photo-degradation [61, 62], diaryliodonium photo-initiation [63] for cationic polymerization.

Moreover, the β-diketo moiety of curcumin makes it as a chelating agent for several transition metals, resulting in an enhanced curcumin stability and a reduced toxicity of the metal [60]. This characteristic of metals complexing allowed using curcumin as a sorbent material for aqueous nickel removal [64] and iron sensing probe [65] as well as a pH and CO_2 sensing [66, 67] and monitoring liposome phase transition temperature [43] .

D. Fluorescence

Fluorescence is a simple highly sensitive luminescence technique based on photo-exciting a molecule and collecting emitted light in return. It is used in several field ranging from biotechnology, DNA sequencing, to bio-sensing, molecular interaction and cell imaging…

The first reported fluorescence application goes back to 1565, where wood extract from lignum mephriticum renders water blueish and therefore used to detect counterfeited wood [68].

In 1800's, several people have reported their observation on minerals and the way they transmitted and reflected colors, but they failed to explain it and attributed it to light scattering [68].

That was until 1852-1853 that Stokes used the term fluorescence, and concluded that the emitted light was always at a longer wavelength than the incident light and backed-up Becquerel observation ten years earlier [68].

1. Principal of fluorescence

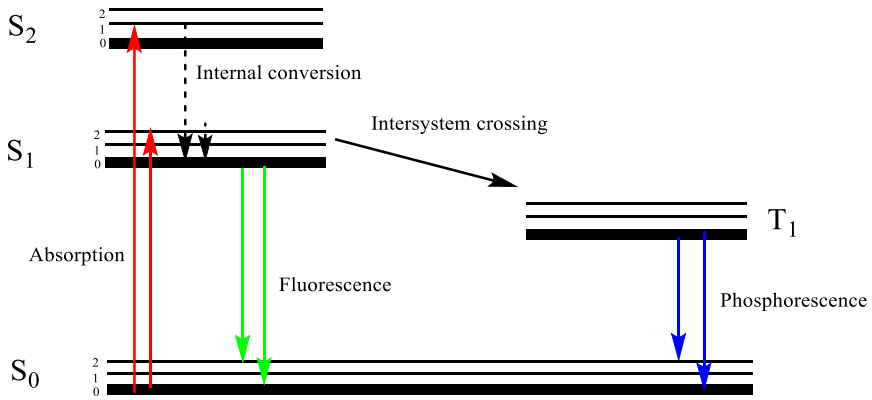

Figure I.3 Jablonski diagram

Fluorescence process can be best explained by Jablonski diagram as shown above. Right after light absorption (10^{-15}s), the molecule relaxes and return to the lowest vibrational level of the first excited state (10^{-12}s), the process is known as internal conversion (IC).

Fluorescence occurs when the energy of the system returns from the lowest vibrational level of the first excited state to ground state S_0 (10^{-8}s), whereas

phosphorescence is due to an intersystem crossing (ISC) from the first excited S_1 state to a triplet state T_1, followed by a forbidden transition to the ground state S_0, a process characterized by a delay in the emission and a higher emission wavelength compared to fluorescence.

2. Quantum yield and life time

Fluorescence quantum yield (ϕ_f) is defined as the ratio of fluorescence rate (k_f) over the radiative and non-radiative rate (k_{nr}) processes or more simply as the number of photons emitted by fluorescence over the total number of photons absorbed.

$$\Phi_f = \frac{k_f}{k_f + k_{nr}} \quad (1.2)$$

The non-radiative processes include the internal conversion, intersystem crossing, heat conversion, photo-bleaching, collision. After excitation an excited molecule (S*) may undergo several of the following possibilities.

$$S^* \rightarrow S + h\nu_f \qquad k_f$$
$$S^* \rightarrow T^* \qquad k_{ISC}$$
$$T^* \rightarrow S + h\nu \qquad k_{phos}$$
$$S^* \rightarrow S \qquad k_{IC}$$

Fluorescence life time τ_f , is the time required for the fluorescence intensity to decrease to 1/e its initial intensity, where $\tau_f = \frac{1}{k_f}$. In a real sample, the non-radiative

decay rates should be included for the experimental life time determination, therefore it is defined as $\tau = \frac{1}{k_f + k_{nr}}$ and $\tau = \phi.\tau_f$.

In polar solvent, fluorophore (F) emits at higher wavelength due to the reorientation of the solvent molecules around the large dipole moment of the fluorophore at the excited state lowering by this its energy. This behavior is generally observed in the case of polar fluorophore, but apolar molecules are not sensitive to their environment[69].

3. Quenching

Fluorescence quenching is described as a process by which fluorescence intensity decreases. Mainly two modes of quenching exist: collisional and static quenching.

a. Collisional quenching

It occurs when the fluorophore is in the exited state collides with the quencher. Stern-Volmer plot, F_0/F versus quencher concentration [Q] is linear with a slope $k_q\tau_0$, where k_q is the bimolecular fluorescence quenching constant and τ_0 is the fluorophore life-time in the absence of the quencher.

An important characteristic of collisional quenching is the dependence of the fluorophore lifetime of the quencher concentration.

$$\frac{F_0}{F} = \frac{\tau_0}{\tau} = k_q\tau_0[Q] + 1 \quad (1.3)$$

Moreover, temperature elevation raises the diffusion and hence an increase in the collision rate and consequently an increase in the quenching rate.

b. Static quenching

This kind of quenching happens when the fluorophore bound to the quencher, forming a stable non-fluorescent complex in the ground state.

$$F + Q \rightarrow FQ \qquad K_s = \frac{[FQ]}{[\mathrm{F}][\mathrm{Q}]} \quad (1.4)$$

And the Stern-Volmer plot becomes $\frac{F_0}{F} = k_s[Q] + 1$.

Unlike collisional quenching, the lifetime of the uncomplexed fluorophore is not affected, and a raise in the temperature would result in a dissociation of the complex formed and a decrease in the fluorescence quenching rate.

Since both static and collisional quenching have a linear Stern-Volmer plot, life time measurements are considered to be an easy method to distinguish between them

E. Aims

Self-assembly and aggregation behavior plays an important role in drug delivery materials science and sensing applications. In chapter II of this work, the aim is to study the aggregation behavior of chitosan oligosaccharide lactate, which is a slightly modified short chain chitosan polymer. The method employed will be largely fluorescence techniques (using both extrinsic fluorescence of COL and external probe molecules like pyrene and curcumin) with support from electrical conductivity

measurement and SEM. In this chapter influence of ionic strength, hydrophobic salt, etc. during self-assembly process will be investigated. Interaction of curcumin, a representative hydrophobic drug molecule, with COL will be unearthed in pre-aggregated and nano-aggregated form. The partition of curcumin into COL will be quantified and binding constant of curcumin with the nano-aggregated form of COL will be estimated in different temperature to understand thermodynamics of interaction.

Analytical specificity in fluorescence probe based method has long been an intriguing topic that plays a crucial role during estimation for targeted biomedical species. Although enzymatic reaction, base stacking (aptamers) and antigen-antibody linkers are few possibilities, each of these possibilities has their own limitations and gets influence by foreign interference. The other way of addressing such problem could be tuning the probe molecule by using emerging nanotechnology, such as nano hybrid structures. In chapter III, the objective is to synthesize curcumin integrated COL assembled silica hybrid nanoparticles for the determination of cholesterol. These nano hybrid particles will be characterized by XRD and electron microscopy. The selectivity of the synthetic hybrids particles will be compared to that of curcumin, in the presence of several metallic ions, electrochemical and hydrophobic interferent. Following a calibration curve for cholesterol concentration will be built ranging from 2 μM to 10 mM, and the binding ratio NHPs to cholesterol will be predicted.

CHAPTER II

INTERACTION OF CURCUMIN WITH PRE- AND SELF-ASSEMBLED CHITOSAN OLIGOSACCHARIDE LACTATE

A. Introduction

Taking advantages of the positively charged amine groups (below the pKa) and hydrophobic polymeric chain (above the pKa), chitosan can interact with charged electrolyte or hydrophobic molecule to form a polyelectrolyte (below the pKa) or polymeric (above the pKa) complex. These complexes are formed mainly by electrostatic and/or hydrophobic interaction between polymer backbone and the charged/hydrophobic entity of interacting molecule [70, 71]. Chitosan oligosaccharide lactate (COL) is a minor modification form, having a shorter chain and lactate as a counter ion, to enhance water solubility and its application in drug delivery, nanotechnology and biomedicine. Interesting physicochemical properties of COL are directly connected to the intra- and intermolecular associations between the hydrophobic functionalities in aqueous solution within a certain concentration range. However, COL's behavior in solution and interaction with drug molecule has not been explored. Curcumin is a hydrophobic molecule containing β- diketone group that tautomerizes between its enol and keto structures. It has also two phenolic groups in the two different benzene rings. Though interaction of curcumin with liposomes and micellar system is strong, where it often gets buried into the hydrophobic cavity of liposomes/micelle [43, 72], study on polymer-curcumin interaction is limited.

Application of curcumin as a molecular probe to study micelle [72], liposomes [43], and heterogeneous systems [73] is widely getting realized. It is also being used for

fluorescence nano-sensing [74, 75] and synthesis of nanoparticles [45, 76] along with polymer matrix. Thus, it is vital to understand interaction of curcumin with COL keeping the applicability of both curcumin and COL in drug delivery, biomedical and nanotechnological applications. In this work, we have investigated self-assembly and aggregation behavior of COL in solution and interaction with curcumin, a representative hydrophobic drug molecule. The association constant, thermodynamic parameters and aggregation behavior during interaction have been quantified. Results on aggregation behavior have been compared to those obtained by electrical conductivity and pyrene fluorescence. Critical aggregation concentration, binding constant, partition coefficient, etc. of curcumin with pre- and nano-aggregated forms of COL are also evaluated and studied by varying ionic strength and bile salt.

B. Materials and methods:

1. Materials

COL, curcumin, pyrene, Cetylpyridinium Bromide (CPB), sodium cholate, sodium deoxycholate and pyrene were obtained from Sigma-Aldrich and used as received. The solvents used were of HPLC grade and also obtained from Sigma-Aldrich.

2. Sample preparation

A stock solution of COL (2mg/ml) was prepared in doubly distilled water. Similarly, stock solution of curcumin and pyrene was made in methanol. The stock solutions of KI, CPB, NaCl, sodium cholate and sodium deoxycholate were separately prepared in doubly distilled water. Dilutions were made as desired. For fluorescence

measurement at different COL concentration, concentration of curcumin was kept constant at 2 μM and that of pyrene was at 1 μM pyrene. It was made sure that the amount of methanol present in the solution was less than 1 % (v/v) and did not affect our measurement. For quenching experiments, COL concentration was maintained constant at 100 μM, similarly curcumin and pyrene concentration was kept at 2 and 1 μM, respectively. The quenchers such as KI and CPB were varied accordingly. For the binding and thermodynamics study, COL was maintained at 100 μM and curcumin concentration was varied from 2 to 100 μM. COL fluorescence was monitored at different temperatures.

3. Instrumentation

Room temperature absorption spectra were recorded using a SCOV-570 UV-VIS-NIR Spectrophotometer. Steady state fluorescence measurements were performed by a Jobin–Yvon–Horiba fluorimeter, emission and excitation slits were both set at 5 nm (except in the measurements for pyrene it was kept at 1 nm), equipped with a 100 W Xenon lamp and an R-928 detector operating at 950 V. A thermostat was coupled to the fluorimeter sample holder and temperature reading was measured by an external thermometer. Time resolved fluorescence were done by Jobin-Yvon-Horiba fluorimeter, using a pulsed diode laser at 282 nm coupled to an R-928 detector operating at 950 V. FTIR spectra were recorded on FT-IR spectrometer Thermo-Nicolet. Morphological characterizations of the aggregate were performed using a scanning electron microscope (SEM), Tescan, Vega 3 LMU with Oxford EDX detector (Inca XmaW20). Briefly, few drops of a chitosan solution were deposited on an aluminum stub, coated with carbon conductive adhesive tape.

C. Results and discussion:

1. Self-assembly and critical aggregation concentration

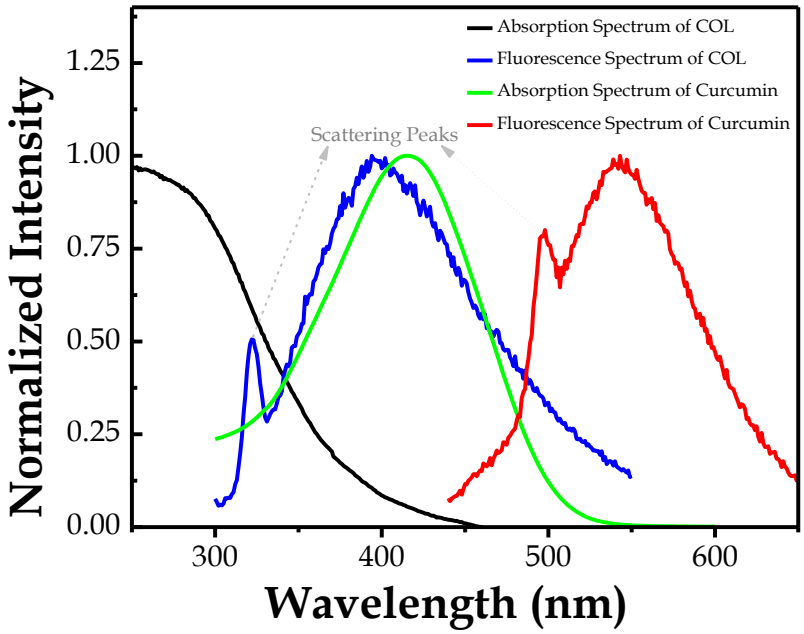

Figure II.1 UV-visible absorption and fluorescence spectra of COL and curcumin

The backbone of COL is made of N-acetylglucosamine entity that absorbs in the UV domain at around 200 nm and of the non-absorbent entity, glucosamine. The UV-visible absorption spectrum of COL is shown in Figure II.1, which gave a broad spectrum ranging from ranging from250 nm to 350 nm. When excited at 290 nm, the fluorescence emission of 100 µM COL was found to be broad in the 300-500 nm wavelength ranges with a maximum at ~395 nm.

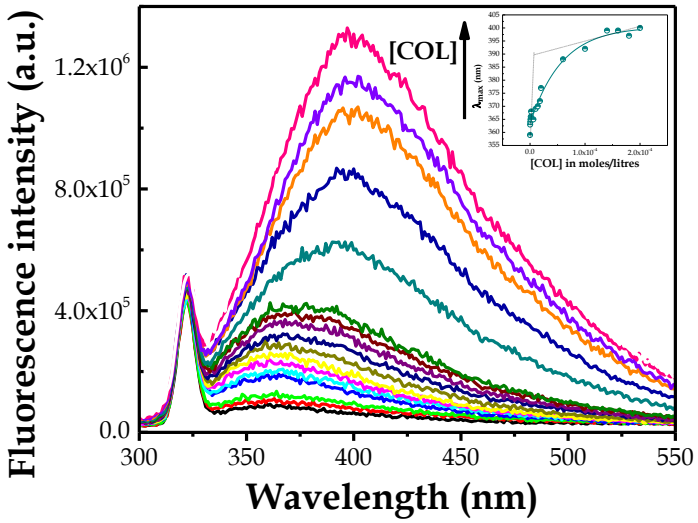

Figure II.2 Fluorescence spectra of COL in different concentration at excitation wavelength 290 nm (Inset: variation of emission maximum)

However, at very low concentration (~600 nM), the emission maxima were located at ~364 nm (see Figure II.2). The fact is that COL emission is solely due to acetylglucoseamine moiety present in chitosan backbone. Thus, at low concentration no major interaction between the acetylated unit and the surrounding is expected, but at higher concentration this interaction cannot be avoided due to self-assembly/folding process of polymeric chain. For example, with increase in concentration of COL from 600 nM to 200 μM the emission maxima exponentially red shifted (inset) and remained constant at ~ 400 nm at higher concentration ranges suggesting there is a change in polarity of surrounding environment of fluorophore (acetylglucoseamine).

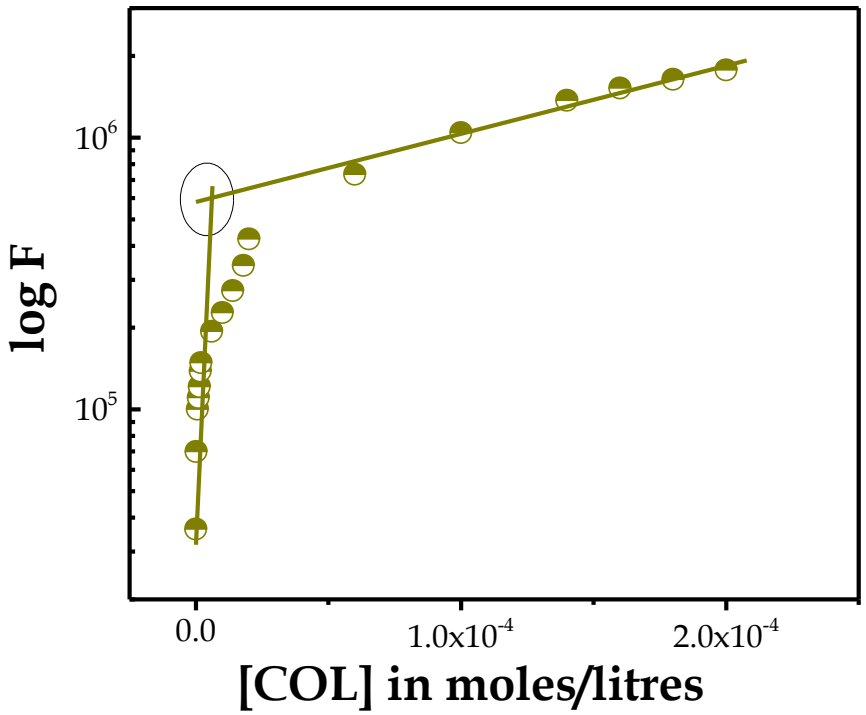

Figure II.3 Logarithmic fluorescence intensity of COL at different concentration

The fluorescence intensity of COL (Figure II.3) also enhanced continuously with concentration but the rate of enhancement was higher in low concentration range than at higher concentration ranges. This is possible when the COL is present in the unfolded/monomeric form at low concentration and at higher concentration it starts aggregating due to self-assembly/folding of monomeric unit and/or formation aggregation of many monomeric units.

Although micellization is a spontaneous self-assembly, but it only occurs above certain monomer concentration known as *critical micelle concentration* (*cmc*) or *critical aggregation concentration (cac)*. This specific concentration can be detected by the change in certain physical properties, such as, conductivity, surface tension, osmotic pressure, etc. of the solution as monomer concentration increases [77].

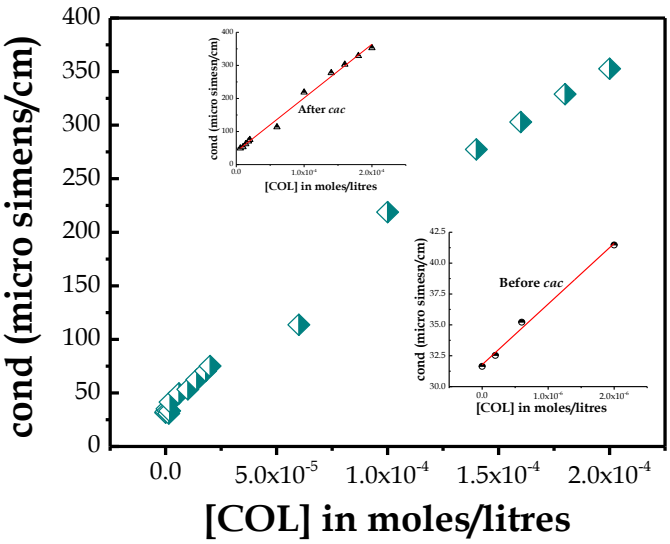

Figure II.4 Change in chitosan conductivity

To understand the nano-aggregation behavior better, electrical conductivity measurement was carried out as a function of COL concentration at room temperature. As can be seen in Figure II.4. the conductivity increased linearly with COL concentration, however, molar conductivity decreased till a particular concentration and remained almost constant afterwards (Figure II.5).

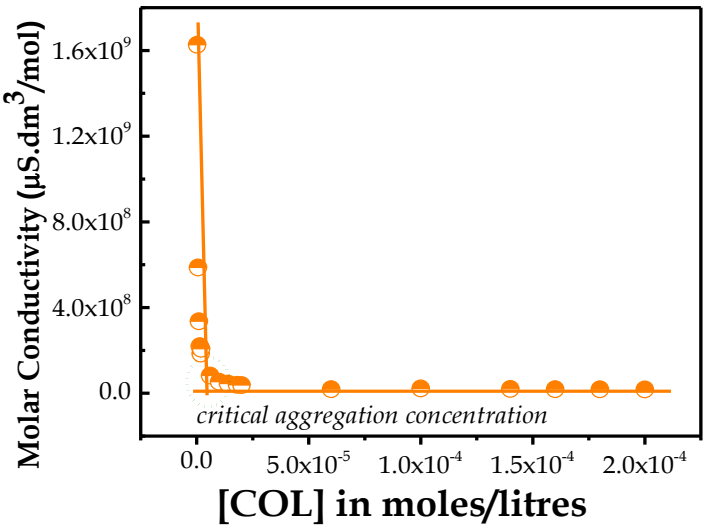

Figure II.5 Chitosan molar conductivity

Since electrical conductivity of water depends on concentration of dissolved salt monomers [78] such linear enhancement of electrical conductivity with COL concentration is expected. The break in molar conductivity vs. COL concentration must have originated from micellization/aggregation of COL [78]. The concentration corresponding to breaking point is *cac*. The estimated value for *cac* was found to be ~5 μM. This value is like the breaking point of two different linear trends observed for fluorescence intensity of COL with concentration.

Further spectroscopic techniques like fluorescence can be used for determining *cmc/cac*. Pyrene is one of the most widely used fluorescence probe[79, 80] to determine *cmc/cac*. To reconfirm the *cac*, pyrene was used as a fluorescence probe to monitor nano-aggregation behavior of COL.

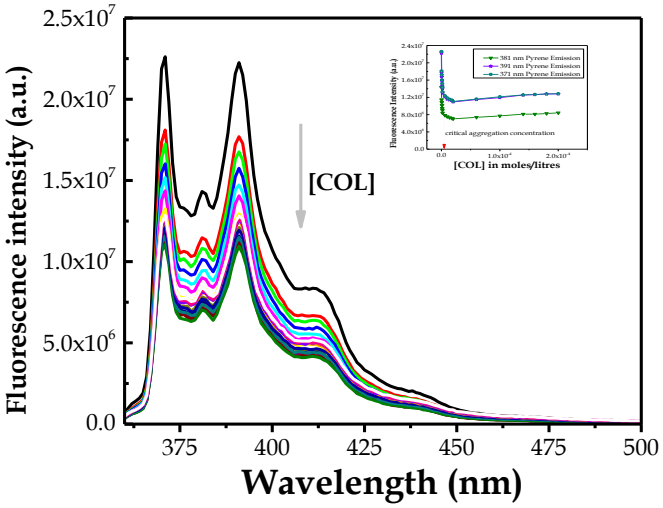

Figure II.6 Pyrene emission spectrum

The fluorescence intensity of pyrene at three different vibrational peaks (at ~371 nm, ~381 nm and ~391 nm) displayed in Figure II.6 was quenched in low concentration of COL (till ~5 μM) and then a negligible improvement was observed in

higher concentration of COL, >5 μM. Based on these two trends, the *cac* was estimated to be ~5 μM (inset), which is same as earlier measured value. In case of pyrene, fluorescence intensity ratio of the first (I_1) and third (I_3) vibronic peaks is often used to estimate micropolarity in heterogeneous media [81]. The I_1/I_3 depicted in Figure II.7 fluctuated abnormally before the *cac*, this is not surprising for COL because in aqueous solution above the pKa value, COL is expected to show the properties of an amphipathic molecule. Unlike surfactant solutions aggregation of COL can occur in many different possibilities like folding/unfolding of monomeric unit as well as self-assembly and aggregation of many COL monomer units together, both are concentration dependent. Such processes may create different microenvironments and influence preferential binding of hydrophobic fluorescence probe like pyrene to different pockets of amphipathic molecule.

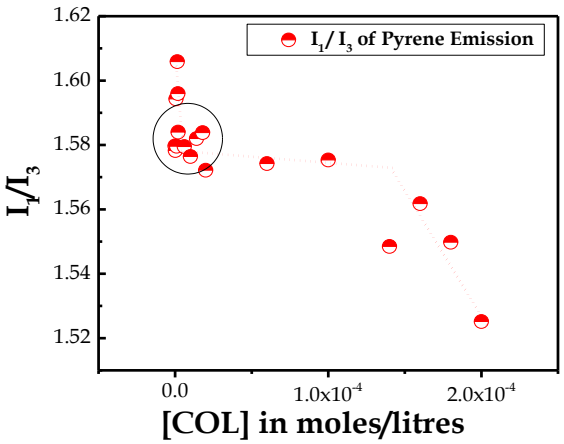

Figure II.7 I_1/I_3 fluorescence maxima of pyrene

Nonetheless, at >100 μM of COL the micropolarity value started decreasing. This observation is similar to sodium dodecyl surfactant solution where a continuous decrease in I_1/I_3 values of pyrene was obtained in post critical micelle concentration

[81] suggesting growth of compact hydrophobic core of COL aggregates due to increase number of COL monomer units participating in aggregation.

Earlier we have also established that curcumin can probe micellization of surfactant molecules [72]. Therefore, in the present case we followed the fluorescence spectra of curcumin in different concentration of COL as depicted in Figure II.8.

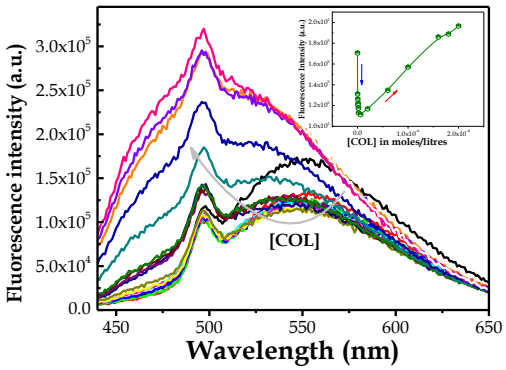

Figure II.8 Curcumin fluorescence spectra, emission intensity (inset)

Remarkably, the fluorescence emission maximum of curcumin illustrated a blue shift (Figure II.9) as COL concentration increases and at very high concentration, >100 μM, it remained constant. The variation of fluorescence maximum of curcumin with COL concentration fitted well with an exponential decay curve.

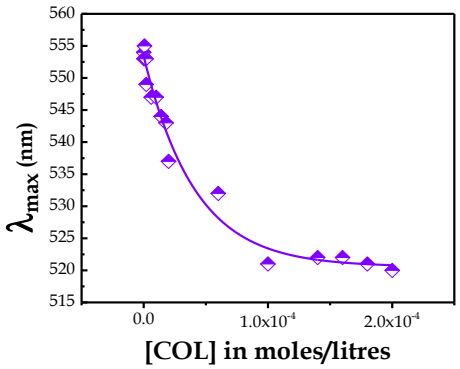

Figure II.9 Emission maximum at different COL concentration

Fluorescence emission maximum of curcumin is sensitive to solvent environment [44, 72] and a blue shift in wavelength scale signifies a more non-polar environment in nano-aggregated form compared to monomeric form of COL. At higher concentration the emission maximum of curcumin was found to be similar to that observed in TX-100 micelle [72]. Likewise, COL quenched fluorescence intensity of curcumin at low concentration. When the COL concentration reached ~5 μM, the fluorescence intensity started recovering and continued to increase at very high concentration, >100 μM of COL. This proves that curcumin, being a hydrophobic probe molecule, could detect hydrophobic microdomains that exist in higher concentration of COL. The two kinds of fluorescence intensity change of curcumin with COL concentration gave an intersection point which allowed the detection of *cac* consistent with the other three earlier measurements.

2. Size and degree of counter ions bound to nano-aggregates

The size and shape of the nano-aggregates was evaluated by SEM images. The nano-aggregates were morphologically found to be spherical in size with the diameter in the ranges 10 to 30 nm as shown in Figure II.10.

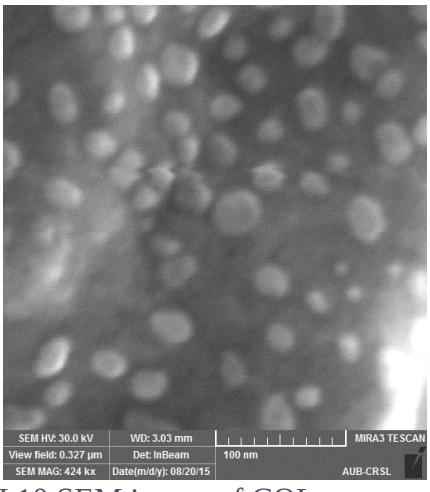

Figure II.10 SEM image of COL nano-aggregates

The size of the nano-aggregates is relatively larger than normal surfactant based micelle formation above the *cmc*, but a polymeric micelle/aggregation may not form the same assembly process that of surfactant units. On the other hand, a careful look of Figure II.4 implies that variation of electrical conductivity with COL gave a relatively higher and lower slope before and after *cac* of COL, respectively. It is anticipated that higher mobility of free monomer ions and counter ions (lactate) offers higher conductivity below the *cac.* On the other hand above *cac,* a decrease in mobility upon aggregation with a fraction bound lactate ions leads to relative reduction in conductivity [78]. To estimate the fraction of bound counter ions to aggregated nanostructures, the change in slopes of conductivity vs. COL concentration in pre- and post-*cac* was used [78, 82]. In our case, the degree of lactate ion dissociation (α) was obtained as the ratio of slopes (k_2/k_1) of conductance vs. [COL] for below (k_1) and above (k_2) *cac.* The degree of lactate ions bound to COL aggregates was calculated to be ($1-\alpha$) and the value was estimated as 0.67, which is similar to reported values for various other micelles [82].

3. Distribution of drug

Fluorescence quenching studies on polymer bound fluorescence probe by external quencher molecule provide important information regarding distribution and microenvironment. In the present case two different well-known quenchers, one hydrophilic KI [83] and another hydrophobic CPB [84], were applied. Due to negatively charged surface I^- prefers to stay in aqueous phase whereas the 16 carbon unit chain of

CPB easily gets incorporated into the hydrophobic domain, but the positive pyridinium moiety of CPB stays exposed to water interfaces[84].

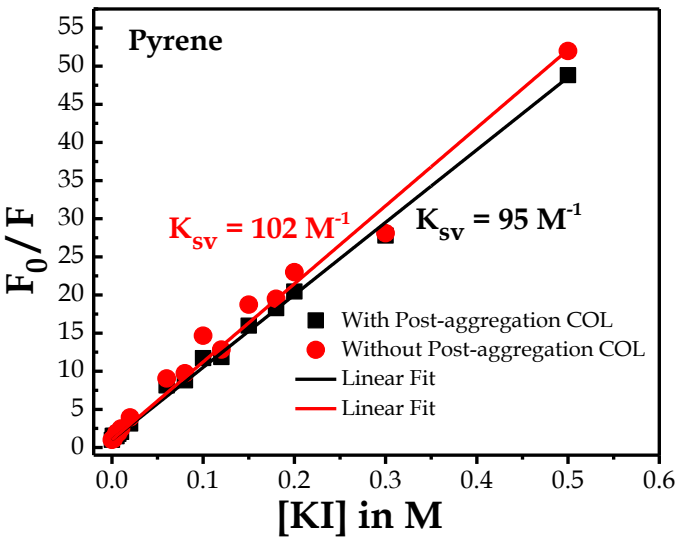

Figure II.11 Stern-Volmer plot of pyrene quenched by KI in the absence and presence of COL nanoaggregates

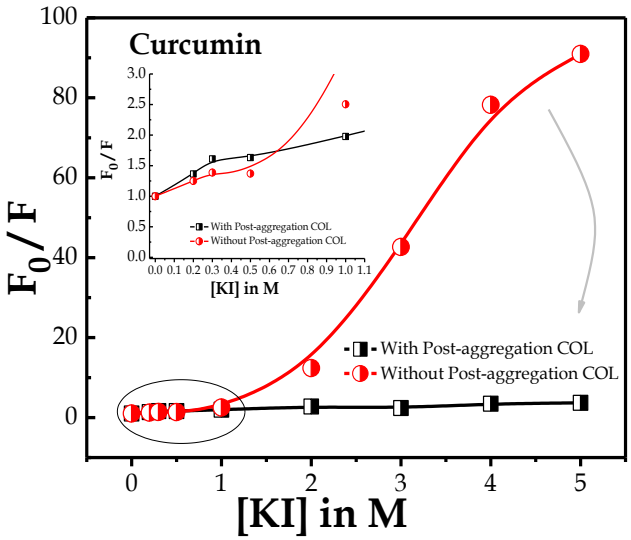

Figure II.12 Stern-Volmer plot of curcumin quenched by KI in the absence and presence of COL nanoaggregates

The fluorescence quenching of pyrene by KI in the absence and presence of nano-aggregated COL (~ 100 μM) is shown in Figure II.11. As can be seen from the

calculated K_{SV} the quenching rate slightly decreased (from 102 to 95 liters/moles) in the presence of COL indicating large part of pyrene remains exposed to aqueous phase. When pyrene was replaced by curcumin (Figure II.12), the quenching rate by KI in the absence and presence was almost similar, but as soon as the KI concentration increased to 1 M the quenching by KI was higher in the absence compared to presence of COL. Further, increase in KI exponentially increased quenching of curcumin by KI in the absence of COL where as in presence of it did not increase. This is not absurd as higher concentration of KI may help in pushing more fraction of curcumin from aqueous phase to hydrophobic domain of COL. This will be discussed further later on.

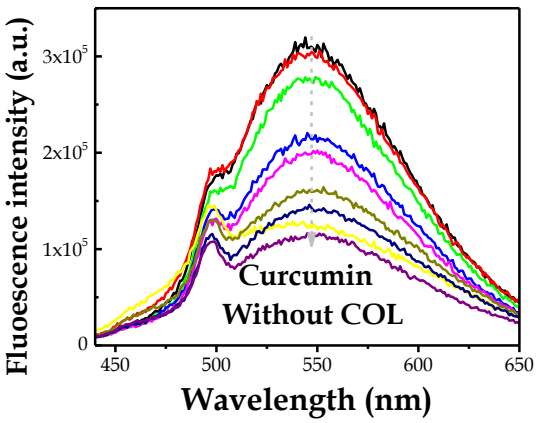

Figure II.13 Fluorescence spectra of curcumin in the absence of COL nanoaggregates in different concentration of CPB

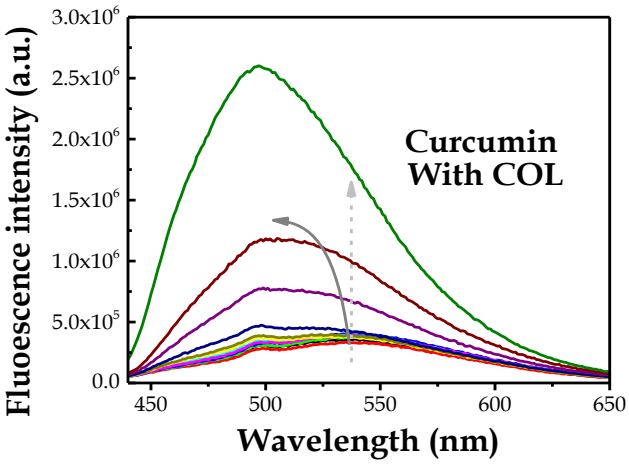

Figure II.14 Fluorescence spectra of curcumin in presence of COL nanoaggregates in different concentration of CPB

In the absence of COL, hydrophobic CPB quenched the fluorescence of curcumin in water without affecting the emission maximum (see Figure II.13), which is similar to pyrene reported in literature [84]. However, in the presence of COL instead of fluorescence quenching, an enhancement in fluorescence intensity and a blue shift in emission maximum of curcumin were observed (see Figure II.14). In contrast, CPB quenched pyrene fluorescence in the presence of COL nano-aggregates, which is in the line of reported literature in heterogeneous system [85]. Thus, there must be something different between pyrene and curcumin while interacting with CPB in the presence of nano-aggregated COL. To explore this behavior, the quenching rate (k) for pyrene by COL in pre-aggregated form (Figure II.15) was compared with that of curcumin. It was noticed that quenching rate for pyrene was about 2.4 fold higher than that of curcumin implying that pyrene has a very strong interaction with monomeric COL compared to curcumin.

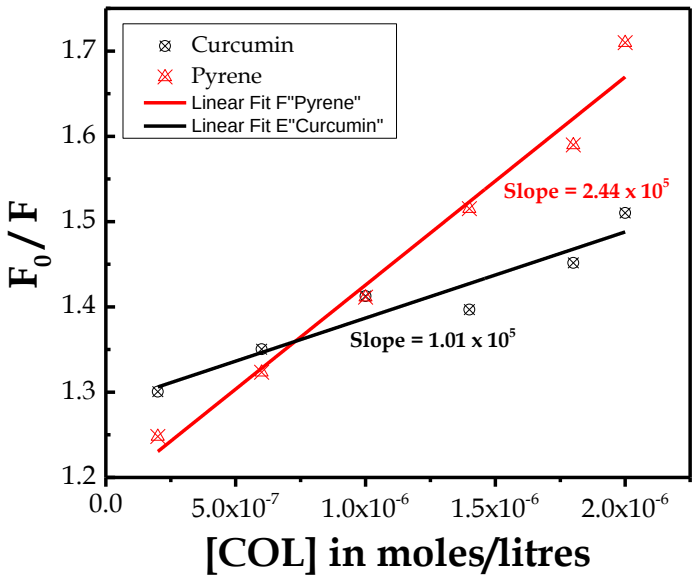

Figure II.15 Fluorescence quenching of pyrene and curcumin by COL in pre-aggregated concentration

Water solubility of pyrene (~0.135 mg/liter) is 2.2 times lower than that of curcumin (~0.3 mg/liter), thus, hydrophobicity of the fluorophore is the main driving force to bring pyrene and COL (monomeric form) much closer compared to curcumin. It is also well known in the literature that the fluorescence quenching of pyrene by CPB is due to electron transfer reaction from pyrene to pyridinium ion [86], which means in COL nano-aggregates pyridinium ion is not closely located to curcumin to have electron transfer reaction unlike in water. This will happen only when COL nano-aggregates would encourage curcumin to align parallel to hydrophobic chain of CPB similar to reported for curcumin in liposomes [87, 88], therefore, as the concentration of CPB increased, curcumin showed a blue shift in the emission maximum when it gets buried more into hydrophobic tail of CPB.

4. Independent hydrophobic microdomains of COL

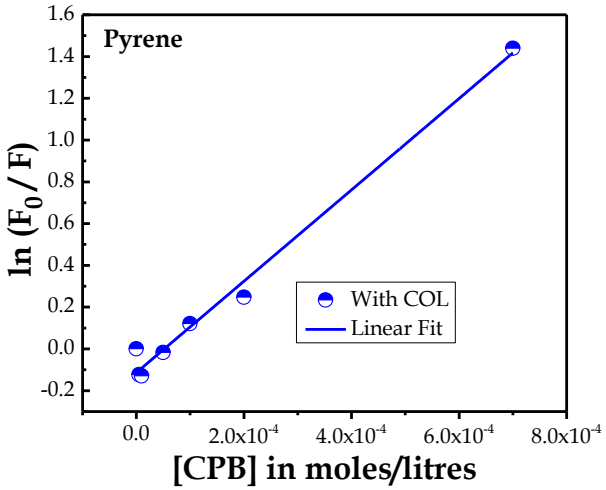

Figure II.16 Plot of ln (F_0/F) vs. [CPB]

Fluorescence quenching of pyrene by CPB in heterogeneous system like micelle etc. [89] has been used to estimate aggregation number. As per the theory by Turro and Yekta [90],

$$\ln \frac{I_0}{I} = \frac{Q}{M} \quad (2.1)$$

Where $M = \frac{C-cac}{N}$ and C is the total concentration of polymer, *cac* is the critical aggregation concentration and N is the aggregation number. In the present case ln (I_0/I) of pyrene vs. [CPB] (Figure II.16) was followed in the presence of COL nano-aggregates (100 μM). The estimated N was found to be 0.21. This value is too small compared to micelles [91]. However, COL has a polysaccharide backbone along with other functionalities. Polysaccharide backbone is hydrophobic in nature and encourages attachment of a hydrophobic molecule like pyrene and subsequently helps in self-assembly process. In such polysaccharide backbone polymeric solution, it is widely reported that instead of a single hydrophobic core multiple numbers of microdomains are formed during aggregation polysaccharide backbone in solution [92, 93]. Within the

boundaries of the exterior lipophobic shell, these microdomains act as physical crosslinks. The construction of such a form in this fashion during self-assembly process can be called as nanogels [94, 95]. The character of multiple numbers of microdomains depends on the concentration of polysaccharide [96], lipophilic group present in the polysaccharide [97] and degree of substitution [97] in the polysaccharide chain. Therefore, in the present case each pyrene molecule may bind to such microdomain pockets and the aggregation number values indeed reflects independent hydrophobic microdomain associated with pyrene, which suggests one polymer chain may form around 5 independent hydrophobic microdomains in the interior of a self-aggregate.

5. Thermodynamic parameters

In an attempt to determine the thermodynamic parameter on association of curcumin with COL nano-aggregates, the fluorescence intensity of COL (100 μM) was monitored at 279, 283, 288, 293 and 298 Kelvin in the presence of different curcumin concentration (2, 5, 10, 15, 20, 40, 60, 80 and 100 μm). The fluorescence intensity of COL at ~390 nm decreased with increase in concentration as portrayed in Figure II.17 for 288 K. Similar trend was observed in all other temperatures.

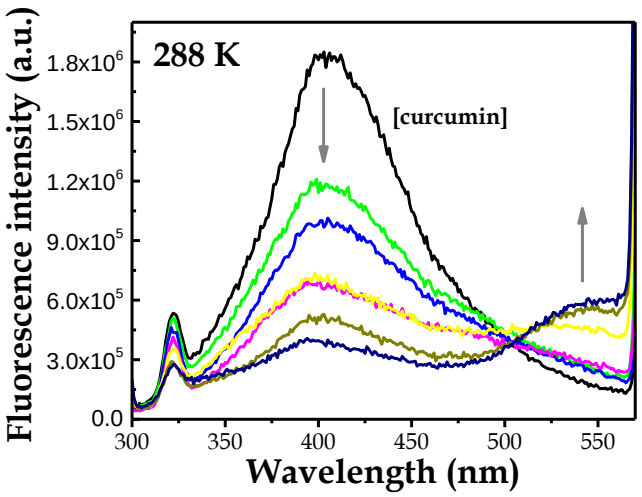

Figure II.17 Fluorescence spectra of COL nanoaggregates in different concentration of curcumin

Interestingly, the fluorescence intensity at around 540 nm increased with curcumin concentration. It can be recalled from Figure II.1, the UV-visible absorption spectrum of curcumin and fluorescence emission spectrum of COL has a strong overlapping region, thus, fluorescence resonance energy transfer (FRET) from COL nano-aggregates to curcumin is possible that can quench the fluorescence of donor COL and enhance the fluorescence of acceptor (curcumin). However, the excited state lifetime of COL in water at room temperature gave bi-exponential decay (Table II.1) with a short component having a lifetime of 1.86 ns (58%) and long component with a lifetime of 7.92 ns (42%).

[curcumin]	τ_1 (B_1) in ns	τ_2 (B_2) in ns	$\tau_{av.}$ in ns
0	1.86 (58%)	7.92 (42%)	4.41
5	1.95 (58%)	7.35 (42%)	4.20
10	1.83 (60%)	7.76 (40%)	4.21
20	1.99 (56%)	7.07 (44%)	4.25
40	1.74 (60%)	8.32 (40%)	4.37
80	1.65 (57%)	8.32 (43%)	4.5

Table II.1 Excited state lifetime values of COL in the presence of different concentration of curcumin

The average excited state lifetime was calculated as 4.41 ns. In the presence of curcumin, the excited state lifetime was not affected appreciably. When FRET mechanism operates, it is expected that excited state lifetime would decrease. In the present case the excited state lifetime variation was negligible.

In addition, quenching mechanism can further be established based on temperature dependence of association constant. Thus, the driving force for the interaction of curcumin with COL was studied by determining the association constant using fluorescence quenching of COL by curcumin. The association constant (K_{asso}) of curcumin with COL could be evaluated as:

$$\frac{F_o}{F} = 1 + K_{asso}[curcumin]$$

$$\frac{F_o}{F} = 1 + K_{SV}[curcumin] = 1 + k_d\tau_0[curcumin] \quad (2.2)$$

where F_o and F were fluorescence intensity in the absence and presence of curcumin. K_{SV} is the Stern-Volmer constant, k_d is bimolecular quenching rate constant and τ_0 is the

excited state lifetime without quencher molecule. Plot of F_0/F vs. [curcumin] gave straight line passing through 1 as shown in Figure II.18

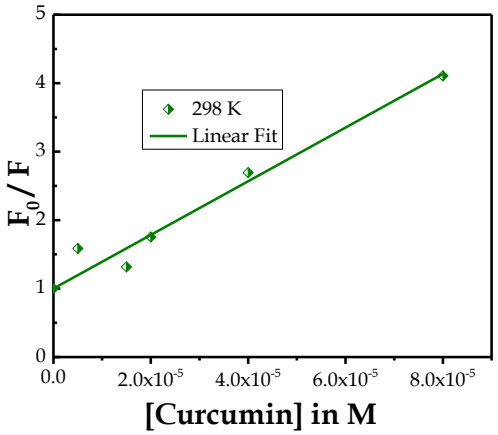

Figure II.18 Plot of F_0/F vs. [curcumin] at 298 K

The association constant for the equilibrium at 279 K was found to be 9.36×10^4 liters/moles. The association constant at different temperature is given in Table II.2

Temperature (°K)	**K_{asso}** (in litre/mole)	**ΔG^o** (in kJ/mol)	**ΔH^o** (in kJ/mol)	**ΔS^o** (in J/K.mol)
279	9.36×10^4	-26.55	-33.98	-27.0
283	8.07×10^4	-26.58		
288	4.42×10^4	-25.61		
293	4.35×10^4	-26.02		
298	3.91×10^4	-26.20		

Table II.2 Association constant and thermodynamic parameters of curcumin binding with COL nano-aggregates

The results gave a significant decrease in association constant or quenching rate constant with increase in temperature suggesting a stronger binding at low temperature. The temperature dependence of quenching rate constant further confirms

that the quenching mechanism is static rather than dynamic. This means the interaction between COL and curcumin is due to ground state complex formation rather than excited state complex formation ruling out any kind of FRET mechanism (despite overlap between absorption spectrum of curcumin and emission spectrum of COL). Therefore, the increase in fluorescence intensity at ~540 nm could be as a result of direct excitation of curcumin at 290 nm, this was further established by measuring fluorescence emission of curcumin in these concentrations at excitation wavelength 290 nm. At room temperature (298 K), the k_d, which is proportional to the sum of the diffusion coefficients for COL and curcumin, was estimated to be 8.9×10^{12} liters/moles.sec (Average excited lifetime value was used for k_d estimation). This value of k_d suggests a diffusion-controlled reaction.

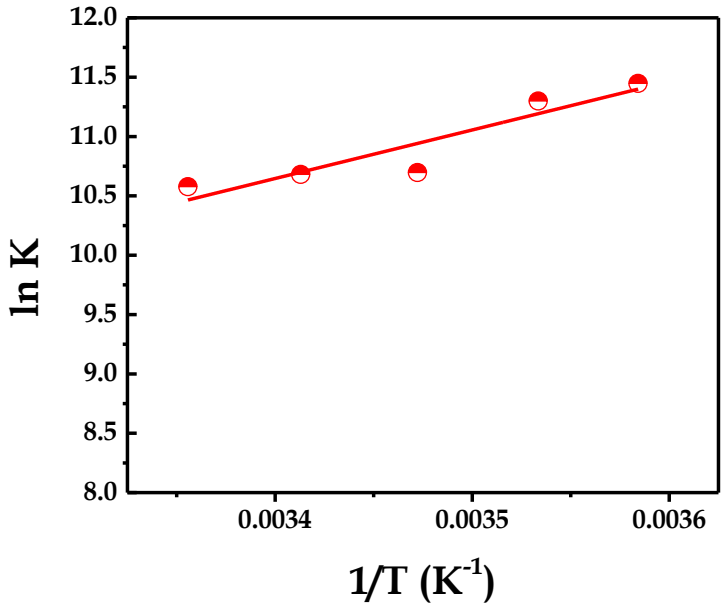

Figure II.19 Plot of ln K_{asso} vs. 1/T

To estimate other thermodynamic parameters such as change in standard enthalpy (ΔH^o) and change in standard entropy (ΔS^o) Van't Hoff equation was applied as:

$$\ln K_{asso} = -\frac{\Delta H^o}{R}\left(\frac{1}{T}\right) + \frac{\Delta S^o}{R} \quad (2.3)$$

where R is the universal gas constant and T is the absolute temperature. Figure II.19 depicts a linear plot for the variation of ln K_{asso} as a function of reciprocal temperature. From this plot, ΔH^o and ΔS^o of association were determined as -33.98 kJ/mol and -27.0 J/K.mol, respectively (see Table II.2). Similar values of negative ΔH^o and ΔS^o have been reported for the interaction of curcumin with liposomes [98] and proteins [99]. These negative values in several protein-ligand interactions have been explained due to introduction of Van der Waal's interactions as consequences of hydrophobic effects [100]. The standard Gibbs free energy change (ΔG^o) was calculated from the binding constant using following equation:

$$\Delta G^o = -RT \ln K_{asso} \quad (2.4)$$

The ΔG^o at various temperatures is summarized in Table II.2. In the present case it was found that ΔH^o for the association is higher than total free energy change suggesting that the association is enthalpy driven. Similar results have been obtained for curucmin-protein system [99]

6. Effect of ionic strength in pre-aggregated form of COL

Effect of ionic strength on the interaction of curcumin with COL was investigated by varying NaCl concentration from 0.25 mM to 10 mM. As control experiments, the fluorescence spectral change of COL in different concentration of NaCl with and without curcumin has been compared in Figure II.20 (see also inset).

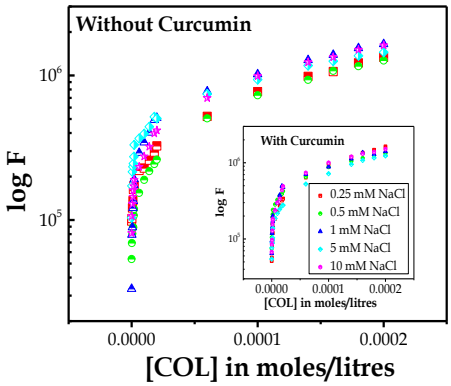

Figure II.20 Variation of fluorescence intensity of different concentration of COL in the presence of NaCl without curcumin, inset shows the same plot in the presence of curcumin

The fluorescence intensity remained the same with and without curcumin (2.0 μM) for various concentration of NaCl indicating curcumin concentration used here has little influence on conformational change of COL. Similarly, the fluorescence intensity of curcumin was monitored for different COL concentration in the presence of NaCl (0.25 to 10 mM). As evident from Figure II.20, the trend in the presence of NaCl was similar to that of without NaCl. The Presence of up to 10 mM of NaCl in the medium marginally lowered the *cac* in the presence of NaCl as given in Table II.3

[Salt]	Critical Aggregation Concentration (*cac*) in moles/litres					
	0 mM	0.25 mM	0.5 mM	1.0 mM	5.0 mM	10.0 mM
NaCl	5.4×10^{-6}	1.5×10^{-6}	1.7×10^{-6}	2.3×10^{-6}	2.5×10^{-6}	2.5×10^{-6}
NaC	5.4×10^{-6}	9.35×10^{-6}	2.45×10^{-5}	4.53×10^{-5}	--	--
NaDC	5.4×10^{-6}	1.7×10^{-4}	--	--	--	--

Table II.3 Critical aggregation concentration of COL with and without different concentration of NaCl and bile salt

Marginal decrease of *cac* in the presence of NaCl is not surprising, it is widely reported in literature that NaCl reduces *cmc* of micelle [101]. However, unlike surfactant systems; in the present case, an increase in NaCl concentration had little effect on the hydrophobic group. To understand it better, the association in the presence of NaCl in pre-aggregated form of COL was evaluated. Since fluorescence intensity of COL in pre-aggregated form was quenched by curcumin in the absence and presence of NaCl, F_o/F vs. [COL] was plotted, which showed a downward curvature indicating that curcumin is fractionally accessible to the quenching effect of COL in pre-aggregated form. In other words, curcumin in solution is distributed into two populations differently interacting with COL. In this case a modified Stern-Volmer plot [69] was used as:

$$\frac{F_0}{\Delta F} = \frac{1}{f_a}\frac{1}{k_{sv}}.\frac{1}{[\text{chitosan}]} + \frac{1}{f_a} \quad (2.5)$$

where F_o and F were curcumin fluorescence intensity in the absence and presence of COL, respectively; $\Delta F = F_o - F$, k_{sv} was Stern-Volmer constant and f_a was the fraction of the initial fluorescence that is accessible to quencher.

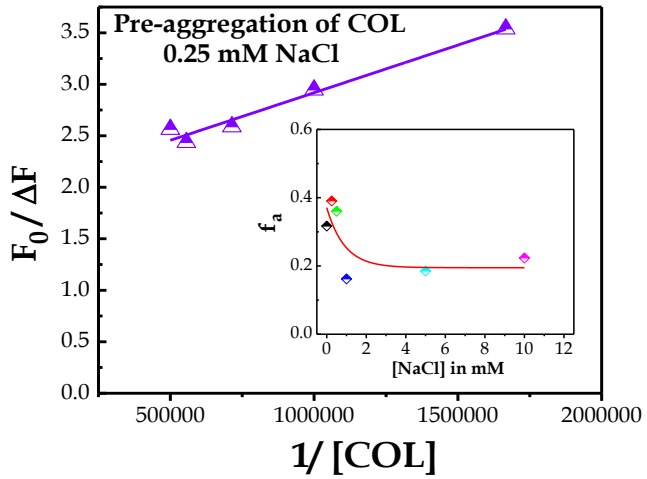

Figure II.21 Plot of $F_0/\Delta F$ vs. 1/ [COL], inset shows f_a vs. [NaCl]

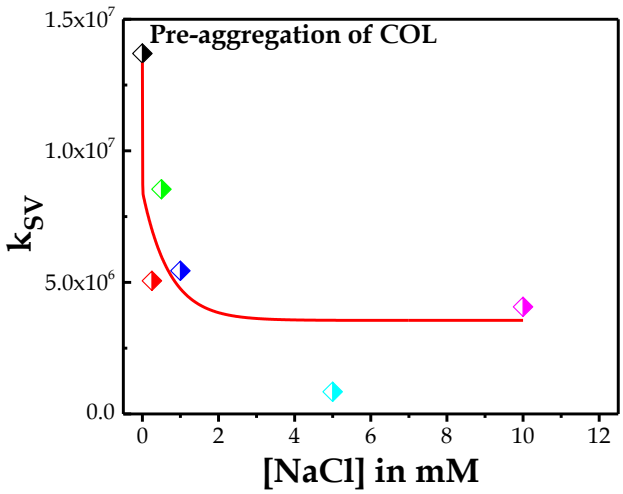

Figure II.22 Plot of k_{SV} vs. [NaCl]

A representative modified Stern-Volmer plot in the presence of 0.25 mM is shown in Figure II.21. The fraction of the initial fluorescence slightly decreased in the beginning and later on remained constant with NaCl concentration (inset of Figure II.21). A similar trend was also observed for k_{sv} (Figure II.22). A decrease in quenching rate indicates that increase in NaCl concentration in the medium discourage interaction of curcumin with monomeric (pre-aggregated) COL, thus, confirming an electrostatic interaction between curcumin and pre-aggregated form of COL.

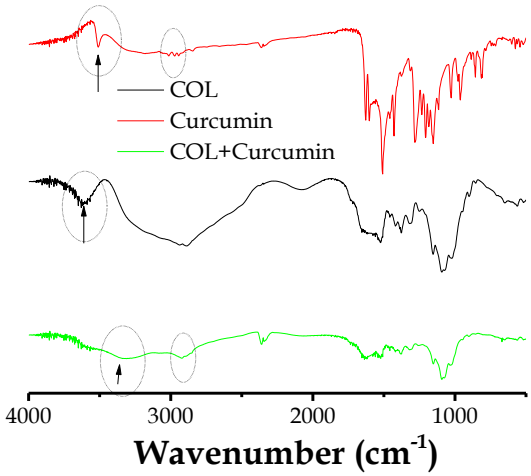

Figure II.23 FT-IR spectra of COL, Curcumin and mixture of COL and Curcumin.

This is further supported by FT-IR spectra measured as depicted in Figure II.23. The phenolic O-H vibration of curcumin was found at ~3510 cm^{-1}, whereas vibration of the free hydroxyl groups of COL was observed at ~3650 cm^{-1}. None of these two prominent peaks were obtained in the mixture of COL and curcumin instead a band was found at ~3315 cm^{-1}. Similarly, the peak at ~ 2973 cm^{-1} due to sp^3 C-H stretching in curcumin could be identified in the mixture of COL and curcumin. The bands due to amide groups at ~ 1560 cm^{-1} and 1404 cm^{-1} were identified in COL, similarly bands at ~1627 and ~1602 cm^{-1} for α-β unsaturated ketone and enol form of curcumin were clearly established. In the mixture, the amide groups of COL and ketone and enol form of curcumin were found to be in the same region. This suggests strong hydrogen bond types of interaction between COL and curcumin.

7. Effect of ionic strength on nano-aggregated COL

To understand partition of curcumin in aggregated form of COL (above *cmc*) compared to aqueous medium, curcumin partition coefficient in COL was determined

based on a procedure reported earlier [43]. Briefly, curcumin fluorescence intensity was monitored at 540 nm after aggregation (above 5 μM of COL) with increasing COL concentration[102]. Curcumin is expected to partition between aggregated COL phase and aqueous medium. The partition coefficient $P_{COL/Water}$, is defined as follow:

$$P_{COL/Water} = \frac{[curcumin]_{nano-aggregate}/[COL]}{[curcumin]_{water}/[water]} \quad (2.6)$$

Where $[curcumin]_{nano\text{-}aggreagte}$, $[curcumin]_{water}$, [COL] and [water] represent curcumin concentration in COL nano-aggregated phase, in the aqueous medium, COL and water concentration respectively. Since fluorescence intensity F is proportional to curcumin concentration bound to aggregated COL $F = \alpha\,[curcumin]_{nano-aggregate}$ and the total curcumin concentration is given by

$$[curcumin]_{water} = [curcumin]_{nano-aggregate} + [curcumin]_{water}$$

Rearranging these equations for application like solubilization, it can be written as:

$$\frac{1}{F} = \frac{55.6}{P_{COL/Water}\ F_0}\ \frac{1}{[COL]} + \frac{1}{F_0} \quad (2.7)$$

where F_0 is the fluorescence intensity when curcumin is in the COL aggregates, and 55.6 mol/L represents water concentration in a dilute medium.

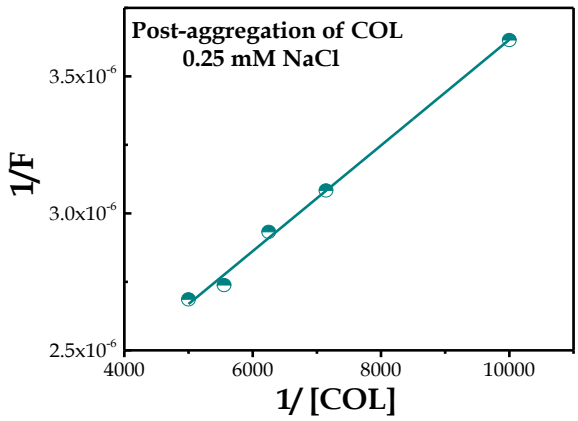

Figure II.24 Plot of 1/F vs. 1/ [COL] for 0.25 mM NaCl

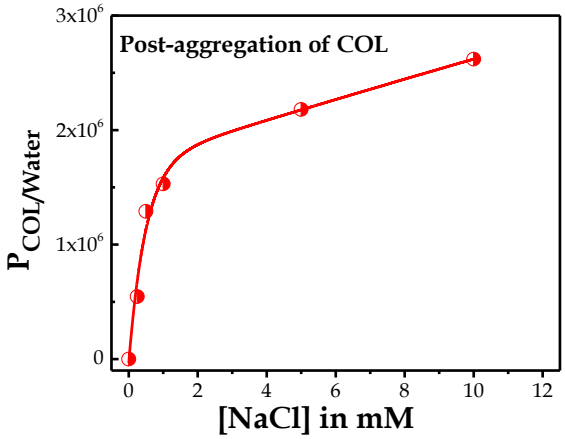

Figure II.25 Variation of partition coefficient ($P_{COL/Water}$) with NaCl concentration

A linear plot of 1/[COL] leaded to estimate $P_{COL/Water}$ from the intercept and slope. As it can be inferred from Figure II.25 and Table II.4, the partition of curcumin into nano-aggregated COL was substantially low, about 1 in 1000 molecules partitioned into COL nano aggregated phase.

[Salt]	**Partition Coefficient ($P_{COS/Water}$)**					
	0 mM	0.25 mM	0.5 mM	1 mM	5.0 mM	10.0 mM
NaCl#	1.23×10^{-3}	5.46×10^{5}	1.29×10^{6}	1.53×10^{6}	2.18×10^{6}	2.62×10^{6}
NaC*	1.23×10^{-3}	8.34×10^{6}	1.79×10^{7}	9.89×10^{6}	--	--
NaDC*	1.23×10^{-3}	2.97×10^{6}	--	--	--	--

Table II.4 Partition coefficient of curcumin in COL nano-aggregates in the presence of NaCl and bile salt.

Earlier fluorescence quenching by KI also confirmed that most of the curcumin/pyrene are accessible to I^-. Thus, the poor partitioning of curcumin into the

nano-aggregated phase is not surprising, possible curcumin is anchored on the surface of nano-aggregates by exposing itself to I^- and aqueous phase. However, increase in NaCl concentration in the medium very remarkably enhanced the partition of curcumin into COL aggregated form, which is consistent with earlier observation at higher concentration of KI. This confirms that in nano-aggregated form the interaction between curcumin and COL is driven by hydrophobicity of COL domains and curcumin.

8. Effect of hydrophobic bile salt

Bile salt has unique properties, as its anion is hydrophobic in nature. Its interaction with heterogeneous environment or aggregation is different from that of ionic salt [73]. It also partition into micelle/membrane and alter its properties [73].

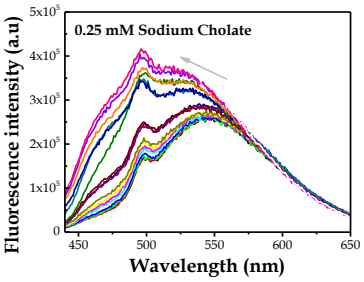

Figure II.26 Fluorescence spectra of curcumin in different concentration of COL in the presence of 0.25 mM sodium cholate

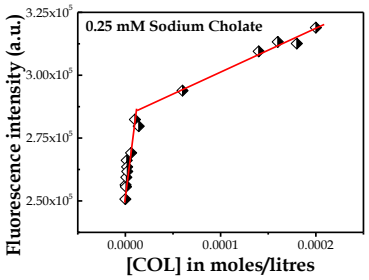

Figure II.27 Change in fluorescence intensity of curcumin in different concentration of COL in the presence of 0.25 mM of sodium cholate

In this case when bile salt containing hydrophobic anion such as sodium cholate was used, the fluorescence intensity of curcumin was not quenched in the pre-aggregated form of COL rather than an enhancement in curcumin fluorescence intensity (Figure II.26) was observed. The initial increase in fluorescence intensity in pre-aggregated form in the presence of sodium cholate is similar to one observed in the presence of CPB earlier and suggests a cooperative interaction between cholate (hydrophobic) and curcumin along with COL that helps in stabilizing the excited state of curcumin. However, the enhancement was much higher in the lower than higher concentration of COL (Figure II.27) and a blue shift in the emission maximum of curcumin was obtained in higher concentration of COL. The blue shift suggests a different microenvironment in higher concentration signifying aggregation of COL.

Based on two different trends in fluorescence intensity, the *cac* was estimated to be 1.7 fold higher than without sodium cholate (see Table II.3). This result is in contrast with that of presence of NaCl where a marginal decrease in *cac* was found. The increase *cac* value in the presence sodium cholate could be hypothesized based on the fact that bulky and hydrophobic cholate group becomes part of aggregation process

along with COL to form large aggregates/micelle, therefore, the nano-aggregates formed in the presence of sodium cholate is different from COL alone and needs higher concentration of COL to accommodate cholate ion in micellization process, whereas in the presence of NaCl the ions remain in aqueous phase and help the hydrophobic domain of COL to come close towards each other to form nano-aggregates in lower concentration of COL. Similarly, at 0.5 mM and 1 mM of sodium cholate the fluorescence intensity of curcumin increased in pre-aggregated form but almost remained constant in post-*cac*.

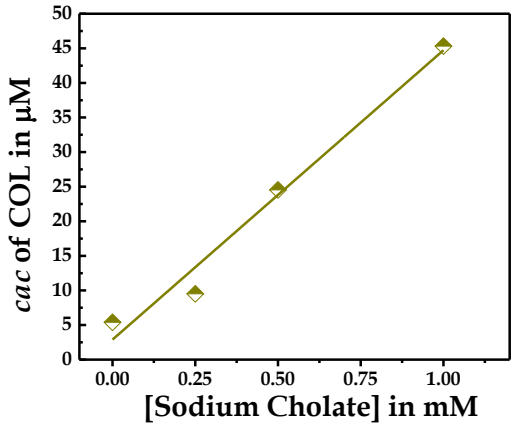

Figure II.28 Plot of cac (critical aggregation concentration) vs. sodium cholate concentration

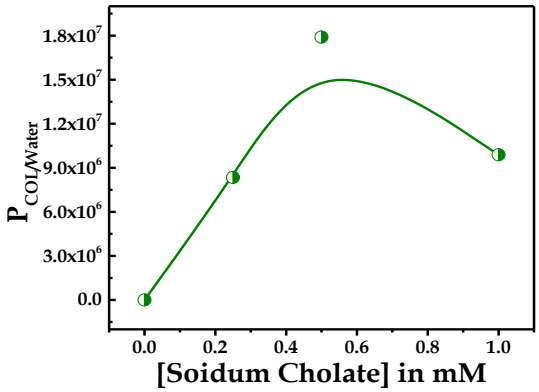

Figure II.29 Plot of partition coefficient of curcumin vs. sodium cholate concentration.

The *cac* value increased linearly with sodium cholate concentration (Table II.3, Figure II.28) suggesting presence of cholate in the solution does not help COL to self-assemble to form nano-aggregates. However, presence of cholate increased partition coefficient of curcumin into pre-aggregated form of COL (Figure II.29) indicating direct interaction of cholate and curcumin.

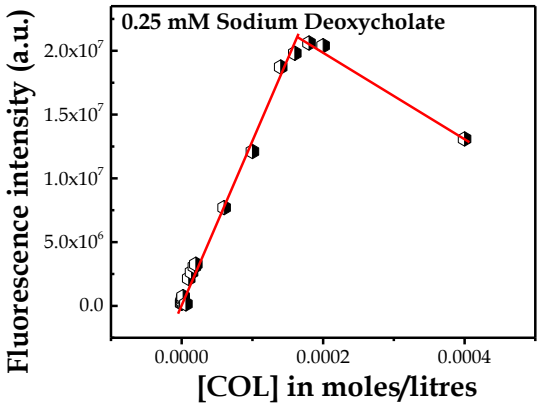

Figure II.30 Change in fluorescence intensity of curcumin in different concentration of COL in the presence of 0.25 mM sodium deoxycholate

When 0.25 mM sodium deoxycholate was used (Figure II.30), the fluorescence intensity of curcumin increased in pre-aggregated form but in post-*cac* the fluorescence intensity of curcumin decreased. Based on the fluorescence intensity alteration, the *cac* was estimated in the presence of sodium deoxycholate as summarized in Table II.3. It was found that the *cac* value increased with sodium cholate concentration. Even while changing from NaCl to sodium cholate to sodium deoxycholate, *cac* value increased. Since deoxycholate is more hydrophobic compared to cholate, as discussed earlier, *cac* is expected to increase.

D. Conclusion

In this chapter, chitosan aggregation behavior and its electrostatic and hydrogen bonding interaction with curcumin is reported in both pre- and post-aggregated form respectively. The effect of inorganic salt enhances the incorporation of curcumin into the hydrophobic domains without affecting the *cac*; and bile salts increase both the partition coefficient and the *cac* of the aggregate

CHAPTER III

ENZYME FREE CHOLESTEROL SENSING USING NANO HYBRID PARTICLES

A. Introduction

Smart polymers having responsive properties have received various interests.[103] Such materials are getting widely utilized in nanoscience and nanotechnology towards sensor designing since two decades[104]. Thus, this field has witnessed fast development and advancement during this period. All types of nanoparticles can be incorporated into different polymeric materials to develop nanoscale sensors. Such nanosensors can be applied in both gas and liquid media analysis[104]; therefore, there are tremendous demands for utilizing nanomaterials as biosensing probes. Based on the hybridization between a target and its complementary probe, various electrochemical and optical methods have been successfully achieved using smart polymers[105]. Water-soluble polymers play crucial role for their applicability in stabilizing nanoparticles, drug delivery, tissue engineering, bioelectronics, biosensing etc[92].Smart polymers that are non-toxic, biologically compatible and chemically versatile are of special interest to create a plethora of formulations and scaffolds for utilization in health care[106]. Chitosan is one such special polymer which self-assemble by changing the pH[107] thus, it has a distinctive combination of properties[108-113].

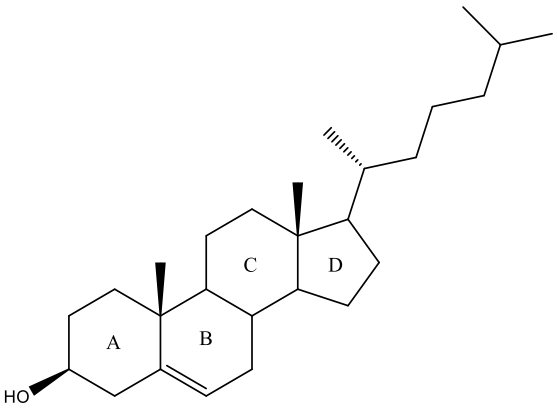

Figure III.1 Cholesterol Structure

Cholesterol is a biomolecule and part of the sterol family characterized by a four-ring structure and a hydroxyl group at the 3-position of ring A, which makes the polar part of the molecule. Cholesterol is found mainly in the animal cell membrane[114] where its presence decreases membrane fluidity[115] and reduces its permeability for polar molecules due to its lateral ordering of neighboring lipids.[116] Cholesterol can be directly synthetized from acetyl-CoA through the mevalonate pathway[117] or it can be imported through dietary[118].The presence of cholesterol in blood at high concentration increases the risk of cardiac and brain vascular diseases[119]. In addition to other conditions, Alzheimer and type-2 diabetes are linked to cholesterol[120]. Moreover few studies have suggested an increase in risk of cancer related to a low level of serum cholesterol[121]. Therefore, determination of cholesterol by rapid, cost-effective and reliable methods is considered very crucial for clinical diagnosis. A total level of 200 mg/dl (5.18 mM) of cholesterol is considered best as reported by the National Institute of Health, and according to the American Heart Association[122]; nonetheless, patient with high cholesterol level exhibits no symptoms therefore the necessity of a periodical clinical test.

Gravimetric, colorimetric and chromatographic techniques have been developed for cholesterol determination in blood and different food sample, but these

methods are expensive and nonspecific. Few of them like GC, requires cholesterol derivatization[123]. Electrochemical-based biosensor for cholesterol determination is getting recently popular by immobilizing cholesterol oxidase (and cholesterol esterase for total cholesterol determination) on the surface of the electrode[27]. Indirect electrochemical method is based on following oxygen reduction current[124, 125] with an O_2 electrode or following either the reduction or the oxidation current of the generated hydrogen peroxide[126, 127] as below.

$$\text{Cholesterol} + O_2 \xrightarrow{\text{Cholesterol oxidase}} \text{4-Cholesten-3-on} + H_2O_2$$

In addition to the indirect detection method, direct electron transfer between the immobilized cholesterol oxidase and the electrode surface has been a subject of study using a carbon modified composite electrodes with an enhanced electron transfer between the ChOX(FAD) deeply buried electroactive species and the surface of the electrode surface[128-131]. However, these enzymes based electrochemical biosensors require a development step to adapt and enhance the surface of the electrode followed by cholesterol oxidase immobilization. A mediator is generally used to lower the detection limit, and the presence of interferences such as ascorbic and uric acid that can be easily oxidized in the same range of H_2O_2 oxidation potential (+0.6 V). In addition, other constraints include optimum working temperature and pH of the enzyme used. Alternatively, fluorescence based methods have been tried using nanoparticles in combination of enzymatic reaction[132]. Kim el al. have reported an enzyme (ChOX) modified CdSe/ZnS quantum dots for cholesterol sensing based of the change in quantum dot fluorescence[133].Since fluorescence methods using enzymatic reaction

are also based on indirect detection of hydrogen peroxide, these methods also suffer due to interference from others substances.

On the other hand there are little report on selective cholesterol sensing using fluorescence probe without enzymatic reaction[134]. This is because of the fact that many fluorescent molecules used as probe have poor selectivity, poor stability and poor sensitivity for the target analytical species. Analytical specificity in fluorescence probe based method has long been an intriguing topic that plays a crucial role during estimation for targeted biomedical species. Although enzymatic reaction, base stacking (aptamers) and antigen-antibody linkers are few possibilities, each of these possibilities has their own limitations and gets influence by foreign interference. The other way of addressing such problem could be tuning the probe molecule by using emerging nanotechnology, such as nano hybrid structures.

In this manuscript, as a proof of concept we propose that COL along with curcumin can be integrated with negatively charged silica nanoparticles to form nano hybrid particles (NHPs), which can be used as a novel analytical technique for cholesterol sensing without enzymatic reaction.

B. Materials and methods

1. Materials

Curcumin, COL, cholesterol, ascorbic acid, Silica LUDOX® HS-40 Colloidal Silica, 6-O-Palmitoyl-L-ascorbic, bovine serum albumin, vitamin E, ascorbic acid, uric acid, urea, glucose, palmitic acid, methyl nonadecanoate, oleic acid, and metal ions such as calcium chloride, magnesium sulfate, zinc nitrate, nickel nitrate, sodium fluoride, lead nitrate, iron (II) sulfate, mercury nitrate, and copper sulfate were obtained from Sigma-Aldrich. All the solvents used were from Sigma-Aldrich

2. NHPs preparation

A stock solution of 1 mg/mL chitosan oligosaccharide lactate dissolved in 1% acetic acid, and a 16 mM curcumin solution in methanol were prepared. 20 µL of curcumin were added to 2 ml of the COL solution and kept under stirring for a couple of hours. After that, 120 µL of the LUDOX silica was added dropwise under continuous stirring, then the whole solution was kept stirred overnight. The formed capsules were left to precipitate, the supernatant solution was discarded and the capsules were dispersed in a 2 mL of distilled water to be used later on.

3. Sample preparation

Different stock solution, each containing an analyte at a concentration of 6 mM dissolved in double distilled water except for cholesterol, 6-O-Palmitoyl-L-ascorbic acid, vitamin E and palmitic acid and the methyl ester (methyl nonadecanoate) were dissolved in methanol. In order to assert the effect of methanol on the fluorescence of the nano hybrid particles, different amount of methanol was used in a cholesterol free medium. For the fluorescence measurement, 100 µL of the dispersed NHPs were added

to 2900 µL of water followed by 50 µL of the prepared analyte solution. Whereas for the cholesterol calibration curve, the 100 µL NHPs solution was dispersed in 2500 µL of distilled water, followed by 400 µL of cholesterol dissolved in methanol at the desired concentration.

4. Instrumentation

Transmission electron microscopy (TEM) measurement was carried out with a JEOL JEM-1400Plus, operating at 120 kV. TEM samples were prepared by casting a drop of the NHPs suspension onto copper grids covered with carbon films. Scanning electron microscopy (SEM) analysis was done using Tescan, Vega 3 LMU with Oxford Edx detector (Inca XmaW20) SEM, where 3 mg of the NC were dissolved in 5 ml of de-ionized water, and few drops of the NHPs suspension were mounted on an aluminium stub, coated with carbon adhesive. After being dried the sample was ready for the SEM analyses. XRD data was collected using a Bruker D8 advance X-ray diffractometer (Bruker AXS GmbH, Karlsruhe, Germany) at 40 kV, 40 mA (1,600 W) using Cu Kα radiation (λ = 1.5418 Å), with a 1.2 mm primary beam slit and 2.0 mm detector slit. The X-ray scans were carried out for 2θ between 5 and 70 degrees at 0.02º increments.

5. Spectroscopic method

FT-IR spectra were recorded using a Thermo Scientific Nicolet iS5 FT-IR Spectrophotometer using KBr pellets. The absorption spectra were recorded using a JASCOV-570 UV-VIS-NIR Spectrophotometer at room temperature. The steady-state fluorescence spectra (excitation and emission) were recorded at room temperature using

Jobin-Yvon-Horiba Fluorolog III fluorometer and the FluorEssence program where the excitation and emission slits width were 5 nm. The source of excitation was a 100 W Xenon lamp, and the used detector was R-928 operating at a voltage of 950 V. The fluorescence lifetime measurements were done using the same instrument except a pulsed diode laser of excitation wavelength 405 nm was used for excitation. Instrumental response (prompt) for lifetime measurement was carried out using colloidal non-fluorescent particles. The decay data were analyzed using Data Analysis Software.

C. RESULTS AND DISCUSSION

1. Interaction of curcumin with polyelectrolye form of COL

At low concentration COL remains in monomeric form due to no major interaction between the acetylated unit and the surrounding. Chitosan has a pKa value in the range 5.5 to 6.5[18] and COL in acidic solution (at pH 2.8) forms polyelectrolyte due to protonation of the amine group.

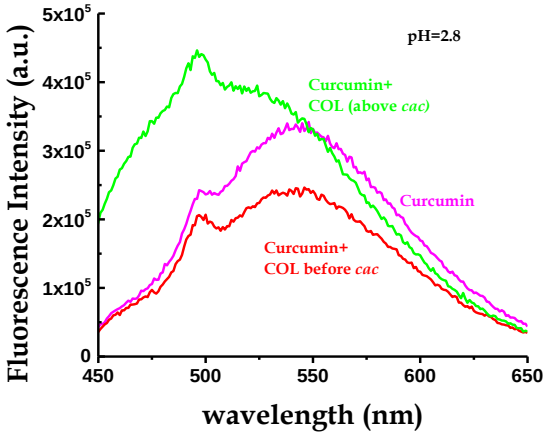

Figure III.2 Fluorescence spectra of curcumin in the presence of COL at above and below critical aggregation concentration (cac)

When curcumin was mixed with COL, fluorescence intensity of curcumin was quenched without affecting the emission maximum (Figure III.2) by monomeric form (below the critical aggregation concentration, *cac*) of COL, however, COL in aggregated form (above the *cac*) recovered the loss in fluorescence intensity of curcumin and further increase in COL concentration enhanced the fluorescence intensity along with a blue shift in the emission maximum of curcumin (see Figure III.2). This suggests interaction of curcumin with COL in polyelectrolyte form is very strong.

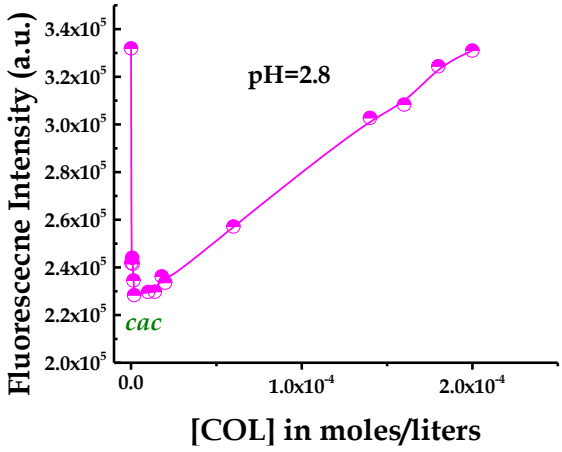

Figure III.3 Fluorescence intensity of curcumin in different concentration of COL

The fluorescence intensity variation of curcumin with COL concentration demonstrated in Figure III.3 could able to locate *cac* of COL, at ~5 µM. This result is similar to that obtained for curcumin in neutral pH condition earlier[140]. The partition of curcumin into polyelectrolyte form of COL (in acidic condition) was evaluated using equation 2.7 [102]:

$$\frac{1}{F} = \frac{55.6}{P_{COL/Water}\ F_0}\ \frac{1}{[COL]} + \frac{1}{F_0}$$

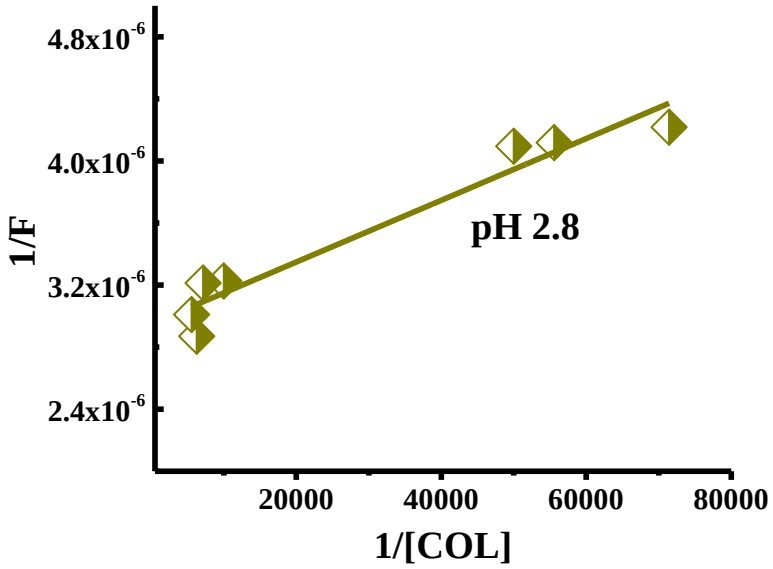

Figure III.4 1/F vs. 1/COL for partition coefficient estimation.

A linear plot of 1/F versus 1/ [COL] (see Figure III.4) leaded to estimate partition coefficient ($P_{COL/Water}$) from the intercept and slope. Interestingly, partition of curcumin into COL could be remarkably enhanced in acidic condition ($P_{COL/Water} = 7.75 \times 10^{6}$) compared to measured earlier in neutral condition($P_{COL/Water} = 1.23 \times 10^{-3}$).[140] This could be due to polyelectrolyte form of COL at pH 2.8, which is similar to association of curcumin with other polyelectrolyte such as poly (allylamine hydrochloride)[141] and poly (L-lysines)[142]. Therefore, for efficient encapsulation of curcumin in COL phase, acidic medium (below pKa) serves the best.

2. Formation of Nano Hybrid Particles

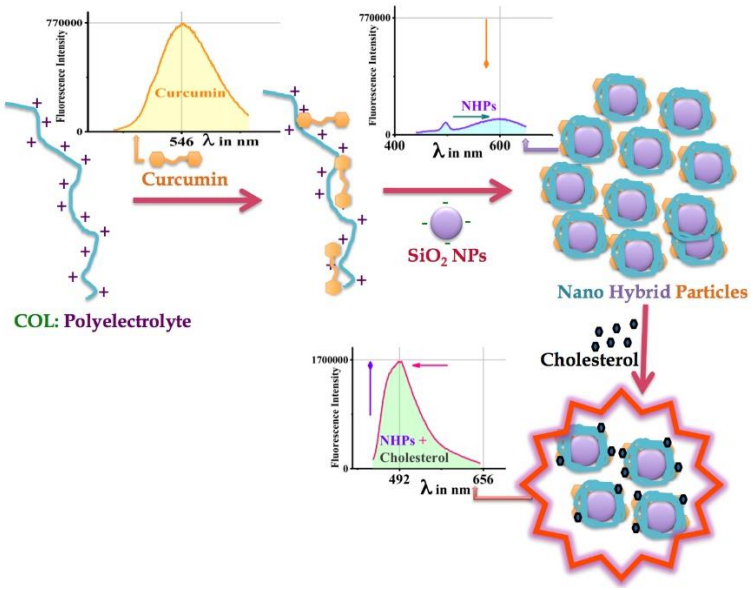

Figure III.5 Illustration of nano hybrid particles formation in the presence of polyelecrolyte (COL), curcumin, silica nanoparticles (SiO_2 NPs) and enhancement in fluorescence in the presence of cholesterol

To enhance stability and partition of curcumin into COL we prepared NHPs by self-assembly method. The self-assembly of COL was achieved using silica nanoparticles (SiO_2 NPs). COL in polyelectrolyte form (in the presence of 1 % acetic acid) was mixed with curcumin under stirring for couple of hours. To this aggregated solution 120 µL of silica nanoparticles of ~20-24 nm size at pH ~9.8 was added drop wise. The obtained cloudy solution was kept for overnight. Note that when less than 100 µL of SiO_2 NPs was used there was no formation of cloudy solution, thus, concentration of SiO_2 NPs plays an important role during formation of NHPs. The formed capsules were left to precipitate and then hybrid mixture was dispersed in doubly distilled water for further characterization and investigation. Due to their overall net negatively charges, SiO_2 NPs assist assembly of positively charged COL (in polyelectrolyte form)

conjugated with curcumin on its surfaces to form spherical NHPs as illustrated in Figure III.5. The size and shape of these obtained NHPs were characterized by SEM.

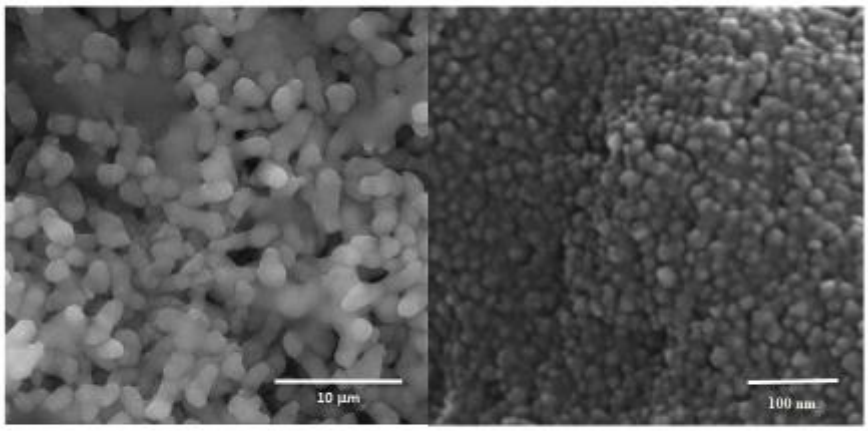

Figure III.6 SEM images of NHPs in aggregated form

SEM image depicted in Figure III.6 indicates shape of these particles is spherical, few elongated and their sizes varies in the ranges 1-3 µm. Earlier we have observed that polyamines cross links in the presence of multivalent anions such as phosphate[141], citrate[143] etc. which subsequently facilitates aggregation of nanoparticles to form spherical microcapsules in the range 0.5 to 4 µm with a thickness of 100 to 250 nm of silica nanoparticles. Interestingly, higher magnification, establishes that in the present case these large particles are aggregated form of smaller and spherical nanoparticles with diameters in the ranges ~25-35 nm, which is different from nano-/micro-capsules obtained earlier.[74, 141-143] This could be possible in two different scenarios. First scenario could be when COL acts as an outer layer to encapsulate aggregated SiO_2 NPs altogether, which can form the core of the structure. However, in this case repulsion from negatively charged SiO_2 NP may not encourage this scenario. And the second scenario could be when COL self-assemble on individual SiO_2 NP

surface to form spherical nano-hybrid particles and then these NHPs congregates in aqueous medium to form large structure due to hydrophobic interaction.

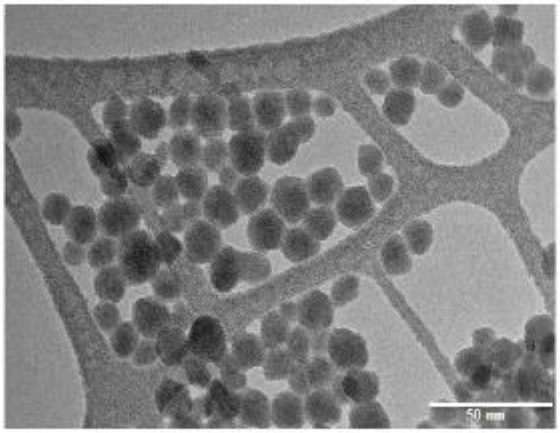

Figure III.7 TEM image of NHPs

To understand this, these particles were diluted and sonicated for few seconds and TEM images were taken. The TEM images shown in Figure III.7 indicate spherical particles of diameter 25-35 nm with a dark core representing SiO_2 NPs and a lighter layer of thickness 4-8 nm over it for COL and curcumin, which proves that the smaller particles are indeed NHPs made up of SiO_2 NP, COL and curcumin.

3. Interaction within NHPs

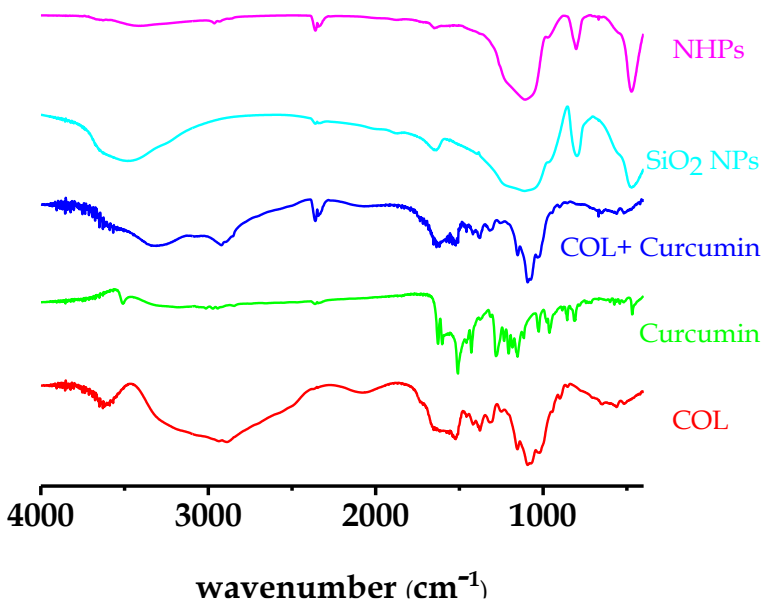

Figure III.8 FT-IR spectra of NHPs, COL and Curcumin

FT-IR spectra of NHPs, curcumin, COL and mixture of curcumin and COL are demonstrated in Figure III.8 . SiO_2 NPs showed an absorption band at ~3482 cm^{-1} due to –OH stretching that shifted to 3415 cm^{-1} after binding and the peak at 1637 cm^{-1} relative to adsorbed water deformation, in addition to absorbance bands at ~ 1108, 973, 798 and 470 cm^{-1} that are the fingerprints of SiO_2 vibration and stretching. The FT-IR spectrum of NHPs is similar to that of silica with a shift to 802 and 472 cm^{-1} of Si-O-Si vibrational peaks and the appearance of a small peak at 2963 cm^{-1} relative to C-H stretching vibration. Unlike to what Lai et al. [144] have reported as an increase in the sharpness of the peak at 1108 cm^{-1} as SiO_2 concentration increases, therefore, upon NHPs formation this peak got sharpened due to the presence of COL. In NHPs two peaks at ~3425 cm^{-1} and 3650 cm^{-1} were found suggesting the interaction between COL and curcumin is different in NHPs compared to in the mixture of COL and curcumin.

The peaks at ~2973 cm^{-1} can be assigned to sp^3 C-H stretching in the case of NHPs, where as in COL and curcumin mixture it shifts to 2966 cm^{-1}

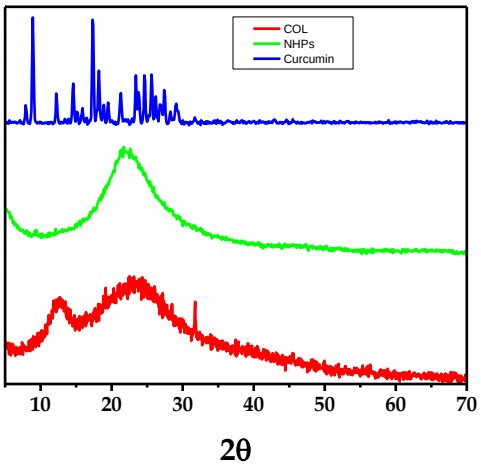

Figure III.9 XRD pattern of NHPs, COL and Curcumin

Figure III.9 shows curcumin XRD pattern exhibiting several characteristic diffraction peaks ranging from 2θ = 5° to 30°, whereas NHPs loaded with curcumin showed only one broad peak with a maximum at 2θ = 21.7° due to the amorphous nature of silica with an alteration of all peaks of curcumin and COL.

4. Optical Properties of NHPs

Curcumin absorbs at around ~425 nm in buffer solution due to strong π(HOMO)⟶π*(LUMO) transition, which masks the weak electronic dipole forbidden n⟶π* band[147-150].Curcumin loaded NHPs have a continuous absorption that is higher at shorter wavelengths, which is largely due to strong scattering of nanoparticles, but the absorption band of curcumin at ~425 nm was identified in NHPs

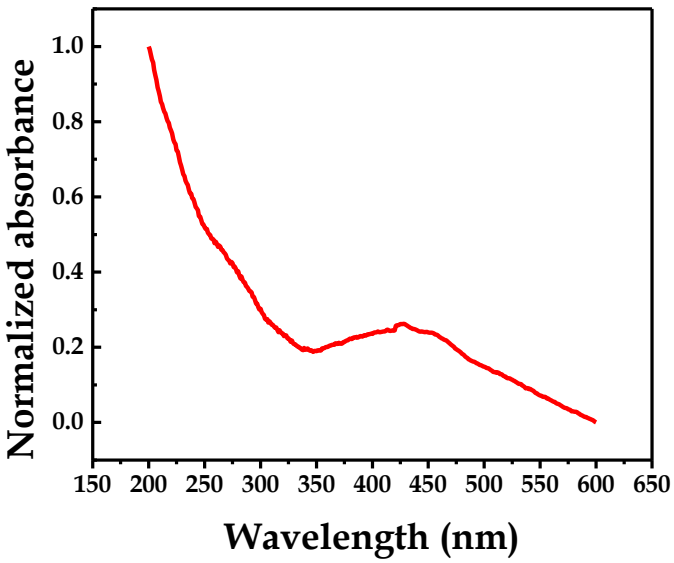

Figure III.10 Capsule absorbance spectrum

Excitation spectrum of curcumin showed a similar peak like absorption spectrum, which is in agreement with the theoretically predicted value for curcumin in enol form[151, 152] no peak at around 355 nm was found for NHPs signifying that curcumin is predominately in enol form in NHPs. However, the excitation spectrum of NHPs was found to be broad with a minor blue shift in excitation maximum (see Figure III.11).

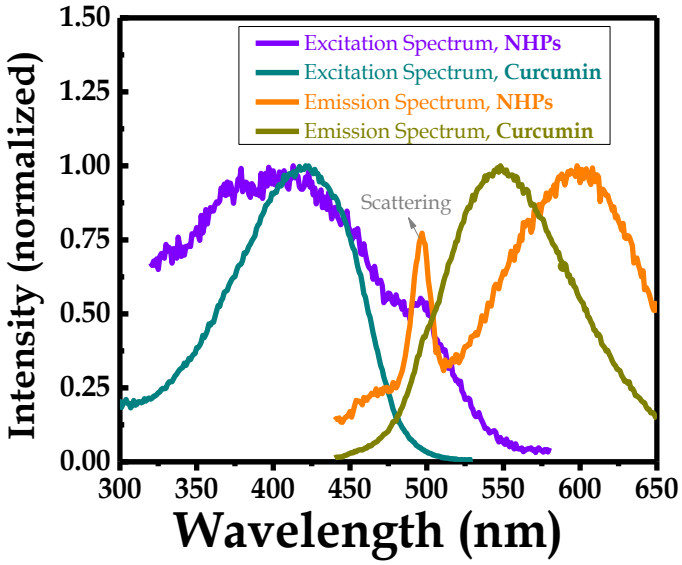

Figure III.11 Fluorescence excitation and emission of NHPs and curcumin in doubly distilled water, the fluorescence intensity has been normalized with respect to intensity at the peak position

The fluorescence emission spectrum of NHPs at excitation wavelength 425 nm was found to be broad, but the emission maximum of NHPs red shifted remarkably, ~50 nm compared to free curcumin. The fluorescence intensity of NHPs was also significantly found to be quenched in NHPs compared to free curcumin in buffer solution. When curcumin was mixed with silica nanoparticles[74], the fluorescence emission spectrum showed a large blue shift from ~550 nm in water to around 495 nm, therefore, the obtained red shift in NHPs is not due to direct interaction between curcumin and SiO_2 NP. Earlier it is also found that while interacting with polyelectrolyte such as PAH[141] and PLL[142],the fluorescence spectrum of curcumin shifts towards shorter wavelength range. While interacting with hydrophobic pockets like in micelle or liposomes, curcumin also shows a blue shift peaked at ~492-510 nm[44], whereas diketone form of curcumin has an emission maximum in lower wavelength range[141]. Thus, the large red shift observed for NHPs excludes any kind

of hydrophobic association or due to keto form of curcumin. In addition, the absorption maximum did not demonstrate a major shift suggesting there is no ground state aggregation that could lower the energy gap between π (HOMO)⟶π*(LUMO) transition to shift the absorption/emission in longer wavelength. Thus, the observed red shift along with reduction in fluorescence intensity could be due to intermolecular energy transfer between curcumin molecules i.e. homo-Fluorescence Resonance Energy Transfer (homo-FRET) or inner filter effects of molecules present in individual NHPs[69]

5. Interaction with Metal Ions

A set of metal ion interferents that are reported to bind with curcumin and affect its emission intensity were prepared and tested against curcumin and the prepared NHPs. Fluorescence intensity of curumin was highly quenched in the presence of Hg^{2+} ion without affecting the emission maximum. 100 µM of Hg^{2+} ion almost quenched all the fluorescence coming out of curcumin (see Figure III.12).

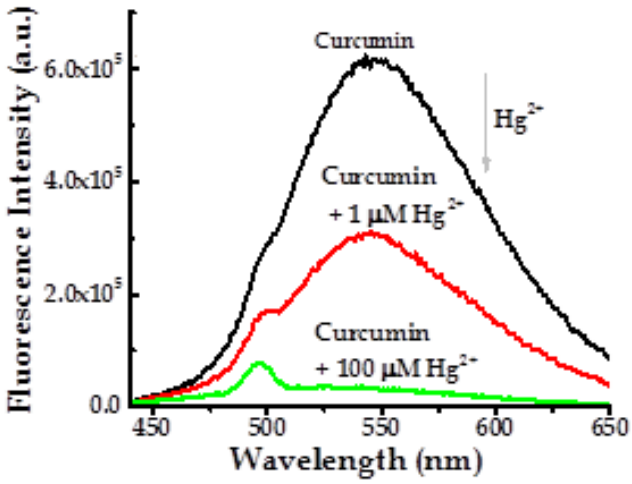

Figure III.12 Fluorescence spectra of curcumin in the absence and presence of Hg^{2+} ion in water

Similar gradual decrease of fluorescence of curcumin by Hg^{2+} ion in DMSO:water (5:1) mixture has been reported earlier[153]. However, when NHPs was used instead of curcumin, there was almost no effect on fluorescence intensity even at 100 µM of Hg^{2+} ion as illustrated in Figure III.13 indicating binding of Hg^{2+} with curcumin is completely blocked in NHPs. Similar results were obtained for Cu^{2+} ions, although the fluorescence quenching rate of curcumin by 100 µM Hg^{2+} ion was ~20 fold whereas by 100 µM Cu^{2+} ion was ~32 fold (see Figure III.14) compared to metal ion free medium.

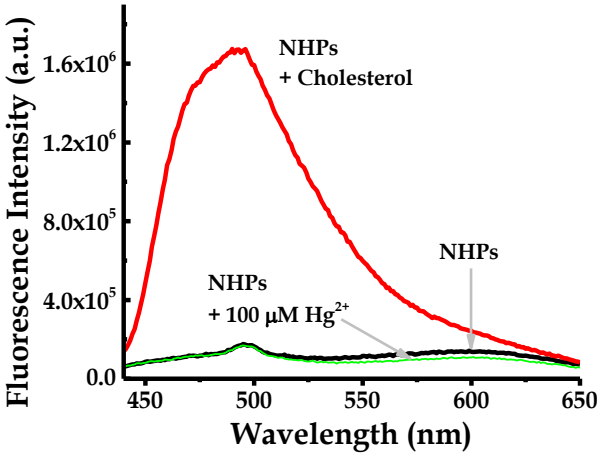

Figure III.13 Fluorescence spectra of NHPs in the absence and presence of Hg^{2+} ion and in the presence of cholesterol in water

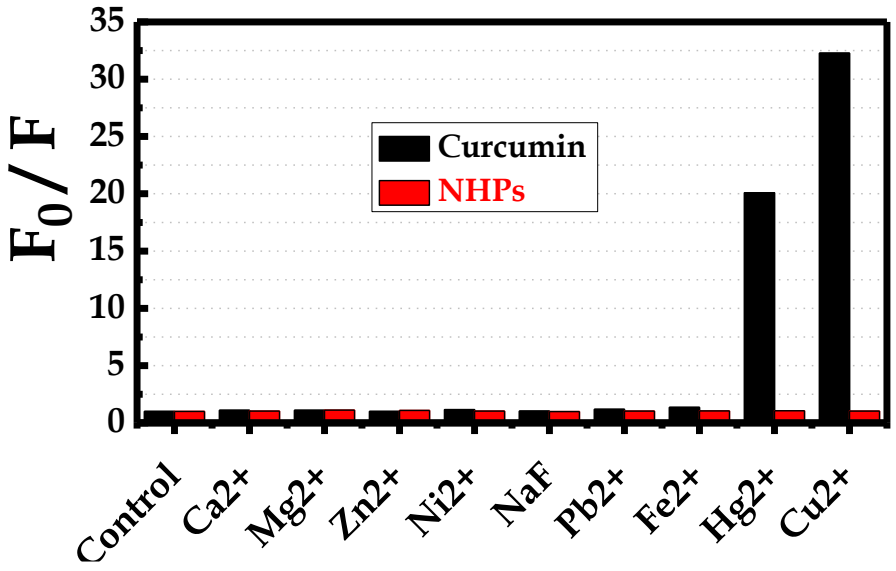

Figure III.14 Comparison of fluorescence quenching (F_0/F) of curcumin and NHPs in the presence of different metal ions. Concentrations of metal ions were fixed at 100 µM.

Metal ions like Hg^{2+} or Cu^{2+} can make complex with curcumin and it has been proposed that Cu^{2+} chelates with keto-enol form of curcumin[154]. When fluorescence of NHPs was measured in the presence of as high as 100 µM of Cu^{2+} ions, there was no appreciable influence on fluorescence intensity of NHPs. The lack of fluorescence quenching of NHPs in the presence of Hg^{2+} or Cu^{2+} ions suggests that keto-enol form of curcumin in NHPs is probably not free to chelate with these metal ions due to interaction of keto-enol form with COL-SiO_2 hybrid structures. In addition, preferential complexation of the metal with the amine –NH_2 function of COL can't be ruled out either [155]

6. Cholesterol Sensing

Once interference from metal was precluded, NHPs were tested for fluorescence sensing of cholesterol. Interestingly, addition of cholesterol remarkably changed the emission maximum and fluorescence intensity of NHPs. A large blue shift of >100 nm was observed in the fluorescence spectrum of NHPs in the presence of cholesterol with a remarkable increase in fluorescence intensity as demonstrated in Figure III.13. When free curcumin was used instead of NHPs a similar blue shift of ~50 nm and appreciable enhancement in fluorescence intensity were found as shown in Figure III.15.

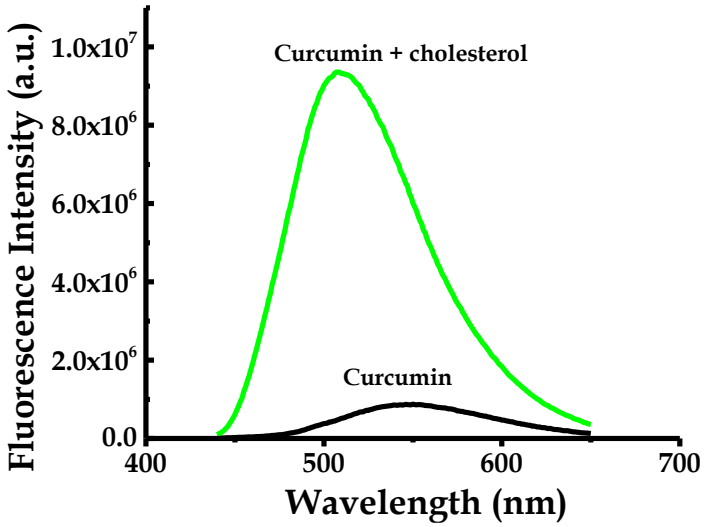

Figure III.15 Fluorescence spectra of curcumin in the absence and presence of cholesterol in water

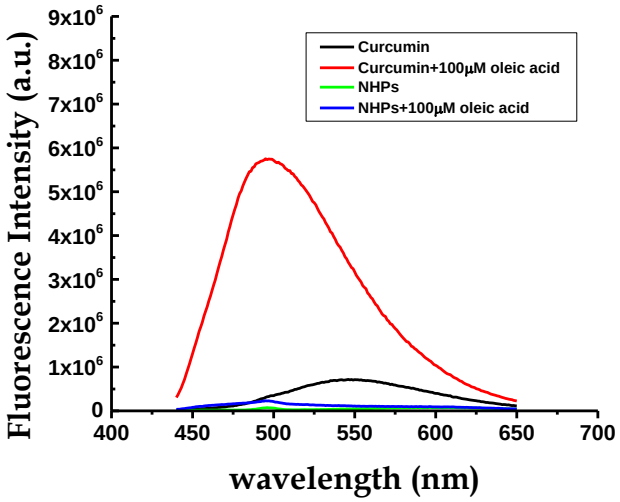

Figure III.16 Fluorescence spectra of NHPs and curcumin in the absence and presence of 100 μM oleic acid in water

The fluorescence maximum and intensity of curcumin is sensitive to hydrophobic pocket[44]. The emission maxima of NHPs and free curcumin were almost identical in the presence of cholesterol centered at ~493 nm. This suggests there is a direct interaction between curcumin and cholesterol in NHPs. The spectral shape and emission maximum of curcumin in the presence of cholesterol is similar to observed for curcumin intercalated in liposomes and non-ionic micelles. Intercalation of curcumin due to hydrophobic interaction with liposomes is relatively well established[44]. We suggest similar kind of interaction between curcumin and cholesterol in NHPs.

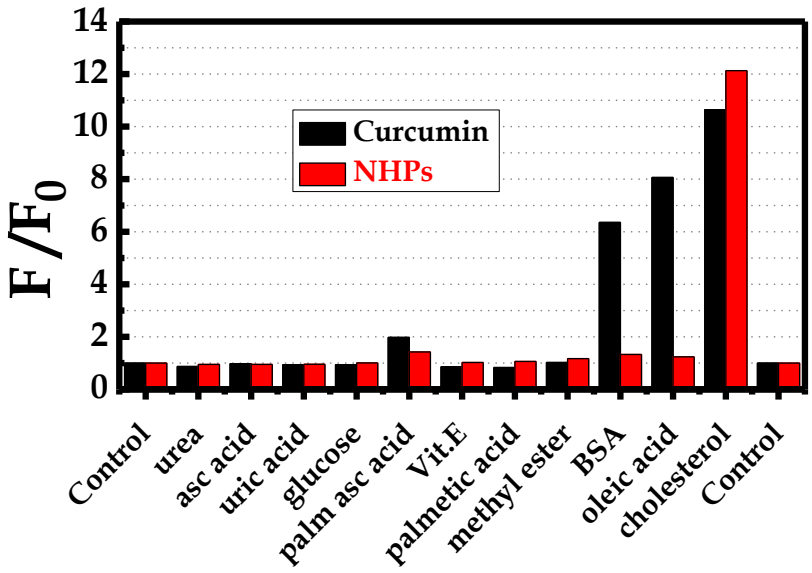

Figure III.17 Comparison of fluorescence enhancement (F/F_0) of curcumin and NHPs in the presence of different biomolecules. Concentrations of biomolecules were fixed at 100 µM except for bovine serum albumin (BSA) where 3.3 µM was used.

To test their selectivity, cholesterol was replaced with another hydrophobic molecule, oleic acid and fluorescence spectra of free curcumin and NHPs were compared. Interestingly, as depicted in Figure III.16, the fluorescence intensity of free curcumin increased 8-fold in the presence of 100 µM oleic acid with a large blue shift (~40 nm) in emission maximum whereas there was a nominal change of <10% in fluorescence intensity of NHPs in the presence of 100 µM oleic acid. Similarly, fluorescence intensity of free curcumin increased 6-fold in the presence of 3.3 µM of serum albumin but that of NHPs was negligible (see Figure III.17). Thus, the interaction of NHPs and cholesterol was special in this case, which is different from that of serum albumin or oleic acid.

The potential interference from various substances was tested. Uric acid, ascorbic acid and glucose that interfere in common electrochemical methods for cholesterol quantification, did not affect fluorescence intensity of both NHPs and free

curcumin as seen in Figure III.17. A noteworthy observation is the differential behavior of curcumin in free form and in NHPs in the presence of lipids (palmitic acid, oleic acid), Vitamin E and bovine serum albumin. Bovine serum albumin, oleic acid and 6-O-Palmitoyl-L-ascorbic acid could interfere during estimation of cholesterol using free curcumin, whereas when NHPs was used interference from these substances could be remarkably minimized apart from suppressing interference from chelating metal ions like Cu^{2+}/Hg^{2+} ion. There was also no interference from other kinds of possible biochemical (Figure III.17) and metal ions (Figure III.14). In addition, the fluorescence enhancement of NHPs was 12 fold higher compared to 10.5 fold for free curcumin in the presence of cholesterol suggesting NHPs enhances both selectivity and sensitivity of cholesterol determination in comparison to free curcumin.

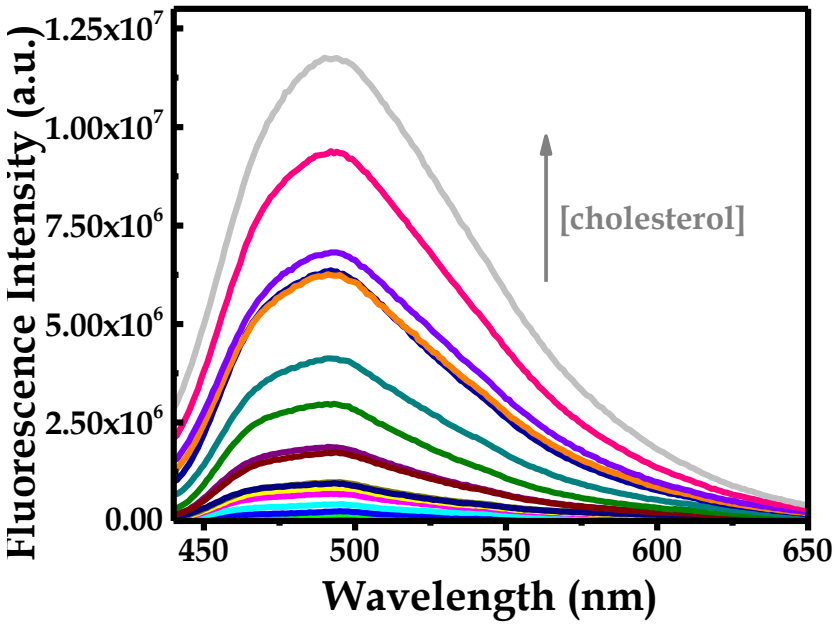

Figure III.18 Fluorescence emission spectra of NHPs in the presence of various concentration of cholesterol

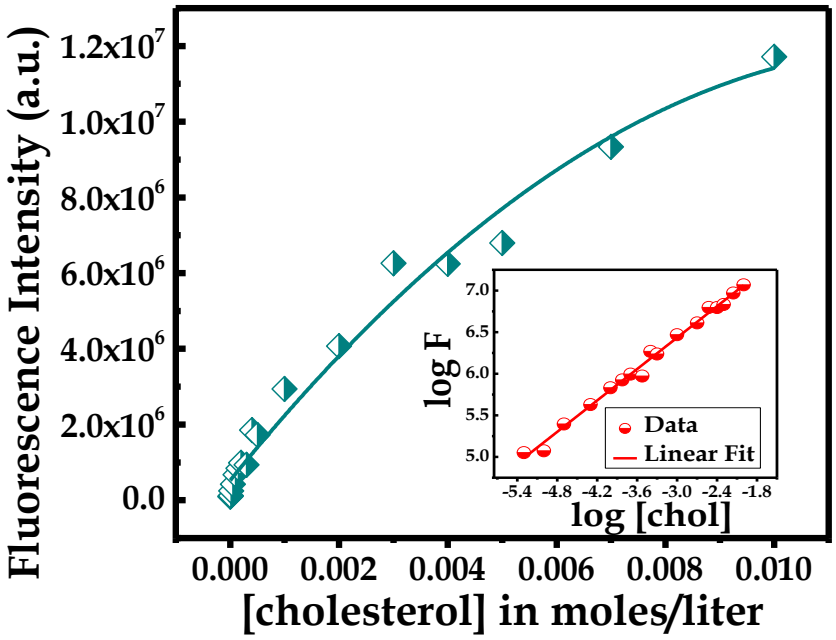

Figure III.19 Calibration curve for estimation of cholesterol by monitoring fluorescence intensity of NHPs, inset shows log-log plot

Comprehending the significance of NHPs for selective and non-enzymatic sensing of cholesterol, the calibration curve for the determination of cholesterol by using NHPs as fluorescence sensing material was established. The fluorescence spectra of NHPs in the presence of different concentrations of cholesterol is shown in Figure III.18, at very low concentration of cholesterol (~2 µM) the emission maximum of NHPs did not change appreciable but 10 µM of cholesterol was sufficient to completely blue shift the emission maximum to ~493 nm, which was not affected by further increase in cholesterol concentration, even at 10 mM of cholesterol. The fluorescence intensity alteration of NHPs with cholesterol concentration is plotted in Figure III.19. As can be seen in the plot, in a wide range of concentration range 0 – 10 mM, the curve showed an exponential growth. The log-log plot illustrated a linear relationship (see inset of Figure III.19). Chang and Ho[156] have used gold nanocluster assisted fluorescent detection for estimation of cholesterol using enzymatic reaction with a linear

dynamic range 2 to 100 µM where has Li et al[132] have reported graphene quantum dots for fluorescence quenching based cholesterol estimation that could detect till 10 µM.

Method	**Materials**	**LOD in µM**	**Linear Dynamic Ranges in mM**	**Reference**
Fluorescence	Graphene QDs-ChOx- H_2O_2	0.08	0.0008-0.01	35
Fluorescence	Au-PVP-ChOx-H_2O_2	1	0.001-0.1	65
Fluorescence	Amplex Red-ChOx- H_2O_2	0.005	0.0005-0.05	66
Fluorescence	Au NPs-β-CD	0.03	0.0003-0.015	67
Fluorescence	Rhodamine B-β-CD-FRET	10	0.01-0.12	68
Electrochemical	G/Ti(G)-3DNS/CS/ChOx	6	0.05-8.0	69
Electrochemical	Pt/TMOS sol-gel/ChOx/p(DB)	-	0.06-3.0	70
Electrochemical	Chox/$PVF^{+}ClO^{4-}$/Pt	-	0.1-5.0	71
Electrochemical	ChOx/AgNPs/GCE	180	0.28-3.3	72
Electrochemical	MWCNTs-ChOxSiO_2-chitosan/PB/GCE	1	0.004-0.7	26
Electrochemical	ChOx-ChE/AuNPs/PTH/GCE	0.6	0.002-1.0	73
Electrochemical	W/ferrocyanide/[ChO/ChEt]	10	0.05-3.0	74
Electrochemical	ChOx/nano-ZnO/ITI	13	0.13-10	75
Electrochemical	ChOx/CS-SnO_2/ITO	130	0.26-10	76
Electrochemical	Nafion/ChOx-Ppy/PB/SAM/Pt	12	0.05-3.0	77
Electrochemical	ZnO@ZnS/ChOx	400	0.4-4.0	78
Fluorescence	Curcumin-COL-SiO_2 NP	2*	0.002-10	Present work

*Minimum concentration that could change the fluorescence signal of NHPs

Table III.1 Comparison of fluorescence and electrochemical sensor performance

Most of the fluorescence probe based cholesterol sensors reported [132, 156-159] using enzymatic reaction or non-enzymatic technqiues are focused in lower detection limit and linear dynamic ranges are in 0.0003 – 100 µM (see Table III.1), which is not of general biomedical diagnosis significance. On the other hand, electrochemical methods reported are in different concentration ranges [27-37] and many of them suffer due to limited linear dynamic range and apply enzymatic reaction as summarized in Table III.1. The best electrochemical method using enzymatic reaction has been reported by Solanki et al.[34] using nanostructured ZnO with a linear

dynamic range 0.13-10 mM with a detection limit of 13 µM. The present fluorescence method has a linear dynamic range 0.002 to 10 mM, which shows wider linear dynamic range than the reported one [28-37, 156-159]. Nevertheless, the present method is not expected to reach lowest detection limit of the methods applied in low concentration ranges (in nM concentration) due to its applicability in higher concentration ranges. For validation, synthetic samples of cholesterol were prepared and the concentrations were estimated using calibration curve obtained from this developed method. The obtained results in the form of percentage of recovery (% of recovery) as summarized in Table III.2 were within 10 %, which is quite acceptable.

Sl. No.	Concentration of Cholesterol Taken in mM	Concentration of Cholesterol Obtained in mM	% of Recovery
1	0.0200	0.022	110
2	0.10	0.109	109
3	1.0	1.13	113
4	7.0	7.16	102

Table III.2 Recovery of synthetic samples of cholesterol using present method.

The association constant of cholesterol with NHPs was estimated using the following equation[160]:

$$log\left[\frac{(F-F_0)}{F_0}\right] = log(K) + n\,log[cholesterol] \quad (3.1)$$

where K and n are the binding constant and the number of binding sites, respectively. F and F_0 are the fluorescence intensity of NHPs at excitation wavelength 425 nm and emission wavelength 500 nm in the presence and absence of cholesterol.

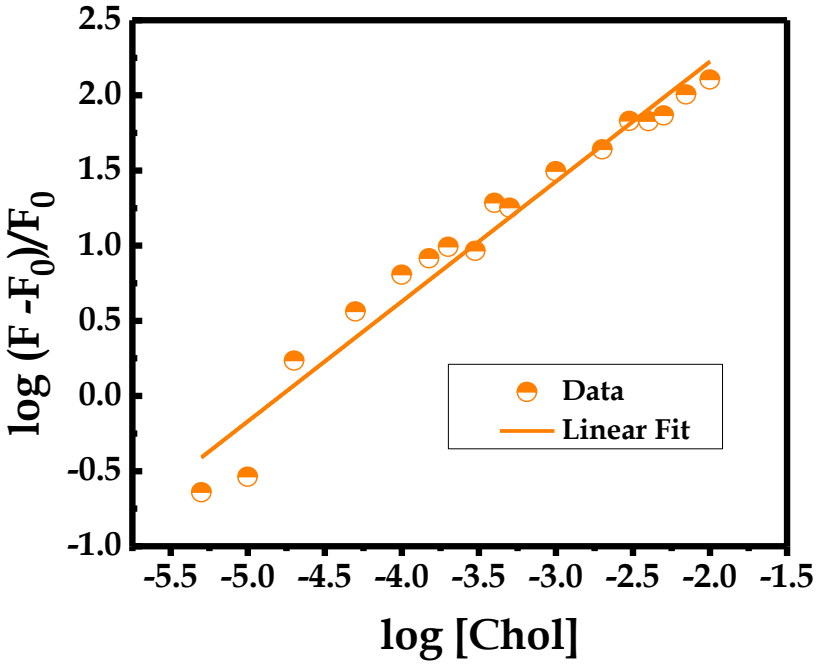

Figure III.20 association constant of cholesterol with NHPs

The association constant of cholesterol with NHPs was estimated as K = 6.60×10^3 M^{-1} and number of binding sites was evaluated to at n = 0.8, which is close to 1 as demonstrated in Figure III.20. The number of binding sites qualitatively suggests not all the curcumin molecules present in NHPs is bound to cholesterol. Since NHPs are much bigger in size compared to size of cholesterol, the possibility of more than one cholesterol molecule binding to NHPs could not be ruled out. It is also important to note that one NHP has multiple numbers of curcumin units and the present n values might be because of binding between cholesterol and curcumin. It is also important to note that one NHP has multiple numbers of curcumin units and the present n values might be because of binding between cholesterol and curcumin.

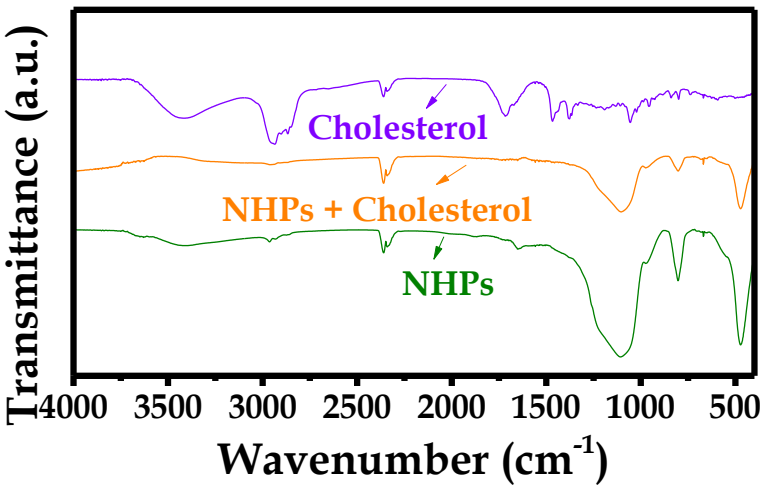

Figure III.21 FT-IR spectra of cholesterol, NHPs and mixture of NHPs and cholesterol

The FT-IR spectrum (see Figure III.21) at ~3415 cm^{-1} for free hydroxyl group of cholesterol[161] and the large band at ~3415 cm^{-1} of NHPs were not clearly identified in the mixture of cholesterol and NHPs. Similarly, band at ~2935 cm^{-1} and ~2867 cm^{-1} due to C-H bond of methyl group of cholesterol was not pronounced in the mixture of cholesterol and NHPs. The band at ~1108 cm^{-1} due to SiO_2 vibration in NHPs shifted to ~1100 cm^{-1} in the mixture of NHPs and cholesterol. These FT-IR results suggest there is some kind of ground state electrostatic interaction through the free hydroxyl group of cholesterol along with hydrophobic interaction between NHPs and cholesterol.

D. Conclusion

Hereby, we are reporting the synthesis silica based nanocapsules using curcumin as a fluorescent probe with differential optical properties. This method has proven to be highly selective for cholesterol with an improved sensitivity compared to other methods previously reported in the literature with a wider dynamic range.

CHAPTER IV

CONCLUSION

In the present work, chitosan self-assembly was studied using curcumin as fluorescent drug molecule. The aggregation behavior of chitosan was found to be not similar to that of ordinary micellar system: formation of independent multiple hydrophobic microdomains. Chitosan intrinsic fluorescence and conductivity measurements have shown a break in the slope value as the concentration of chitosan increase that match that of curcumin and pyrene fluorescence. Rather than a quenching in curcumin emission quenching by CPB in the presence of chitosan; fluorescence enhancement was observed. Meaning that pyrene and curcumin interact differently with the aggregated chitosan The interaction between chitosan and curcumin below cac was found to be different than that at higher concentration: where at low chitosan concentration (monomeric form) curcumin fluorescence is quenched and at higher concentration its fluorescence is restored and accompanied by a blue shift in the emission maxima due to a formation of hydrophobic microdomains

Remarkably, the presence of ionic salt, enhance the incorporation of curcumin into the hydrophobic domain, whereas as at low concentration the presence of NaCl lower the quenching constant suggesting some kind of electrostatic interaction between curcumin and monomeric chitosan. Moreover, the increase in temperature lowers the binding constant (static quenching), with a negative enthalpy change and entropy change. Unlike the case of NaCl, the concentration of bile salt increases the concentration at which chitosan aggregates and a linear correlation between cac and cholate concentration was found. A noteworthy remark is the higher partitioning

coefficient of curcumin in the presence bile salt compared to that of NaCl of the same concentration that can be assigned to a higher hydrophobicity

In the second part, nanohaybrid capsules loaded with curcumin were synthetized in acidic medium by the use of silica nanoparticles by electrostatic interaction. Whereby induce the electrostatic attraction and partition curcumin in the hydrophobic pockets of chitosan. TEM images show that the particles are made of a silica core and an organic shell. Absorbance spectrum of the capsules shows a peak at 425 nm similar to that of curcumin in water but its emission spectrum red shifted to around 600 nm compared to 540 nm for curcumin. Curcumin embedded in the organic layer was protected from chelating with metallic cations that poses a major fluorescence quenching source for free curcumin. In the case of organic interferents, free curcumin fluorescence got enhanced but when integrated into the hybrid capsules, only cholesterol have shown an improvement in capsules fluorescence with blue shift in emission for around 500 nm. This selectivity towards cholesterol lead us to build a double logarithmic linear calibration curve that ranges from 2 µM to 10 mM with an acceptable percent recovery and an NHPs-cholesterol binding constant of 6.60×10^{3} M^{-1} The NHPs were found to be simple, quick and cost-effective, which opens the door to develop novel analytical technique for targeted species using nano hybrid structure without using enzymatic reaction, and to tune analytical specificity, selectivity and sensitivity of probe molecule

REFRENCES

1. Braconnot, M.H., Recherches analytique sur la nature des champignons.
2. Odier, A., Mémoire sur la composition chimique des parties cornées des insectes.
3. Rouget, M.C., Les Comptes Rendus de l'Académie des sciences.
4. Nitar Nwe, Tetsuya Furuike, and H. Tamura, Chitosan from Aquatic and Terrestrial Organisms and Microorganisms: Production, Properties and Applications, in Biodegradable Materials. 2011. p. 29-50.
5. Rinaudo, M., Chitin and chitosan: Properties and applications. Progress in Polymer Science, 2006. 31(7): p. 603-632.
6. M. Rinaudo, G. Pavlov, and J. Desbrières, Influence of acetic acid concentration on the solubilization of chitosan. Polymer, 1999. 40(25): p. 7029–7032.
7. Ki Myong Kim, et al., Properties of chitosan films as a function of pH and solvent type. Journal of Food Science 2006. 71(3): p. E119–E124.
8. M. Rinaudo, G. Pavlov, and J. Desbrières, Solubilization of Chitosan in Strong Acid Medium. International Journal of Polymer Analysis and Characterization, 1999. 5(3): p. 267-276.
9. T. Kean and M. Thanou, Biodegradation, biodistribution and toxicity of chitosan. Advanced Drug Delivery Reviews, 2010. 62(1): p. 3-11.
10. Soichiro Itoh, et al., Development of a nerve scaffold using a tendon chitosan tube. Artificial Organs, 2003. 27(12): p. 1079–1088.
11. Sundararajan V. Madihally and H.W.T. Matthew, Porous chitosan scaffolds for tissue engineering. Biomaterials, 1999. 20(12): p. 1133-1142.
12. Chitosan. 2016 06/06/2016]; Available from: http://www.drugs.com/npp/chitosan.html.
13. P. Fernandez-Saiza, M.J. Ocioa, and J.M. Lagaron, Antibacterial chitosan-based blends with ethylene–vinyl alcohol copolymer. Carbohydrate Polymers, 2010. 80(3): p. 874-884.
14. Yasunori Maeda and Y. Kimura, Antitumor effects of various low-molecular-weight chitosans are due to increased natural killer activity of intestinal intraepithelial lymphocytes in sarcoma 180–bearing mice. The journal of Nutrition, 2004. 134(4): p. 945-950.
15. Caiqin Qin, et al., Enzymic preparation of water-soluble chitosan and their antitumor activity. International Journal of Biological Macromolecules, 2002. 31(1-3): p. 111–117.
16. Lifeng Qi and Z. Xu, In vivo antitumor activity of chitosan nanoparticles. Bioorganic & Medicinal Chemistry Letters, 2006. 16(16): p. 4243-4245.
17. Sweetie R. Kanatt, Ramesh Chander, and A. Sharma, Chitosan glucose complex – A novel food preservative. Food Chemistry, 2008. 106(2): p. 521-528.
18. Davis, S.P., Chitosan: Manufacture, Properties, and Usage. 2011, Nova Science Publishers, Inc, Hauppauge, N.Y.
19. Yan Pan, et al., Bioadhesive polysaccharide in protein delivery system chitosan nanoparticles improve the intestinal absorption of insulin in vivo. International Journal of Pharmaceutics, 2002. 249(1-2): p. 139-147.

20. Rattiya Singhon, et al., Adsorption of Ni(II) ions on colloidal hybrid organic-inorganic silica composites. Colloids and Surfaces B: Biointerfaces, 2012. 93: p. 1-7.
21. P. Miretzky and A.F. Cirelli, Hg(II) removal from water by chitosan and chitosan derivatives: A review. Journal of Hazardous Materials, 2009. 167(1-3): p. 10-23.
22. Muniyappan Rajiv Gandhi and S. Meenakshi, Preparation and characterization of silica gel/chitosan composite for the removal of Cu(II) and Pb(II). International Journal of Biological Macromolecules, 2012. 50(3): p. 650-657.
23. Eric Guibal, Céline Milot, and J.M. Tobin, Metal-Anion sorption by chitosan beads: Equilibrium and kinetic studies. Industrial & Engineering Chemistry Research, 1998. 37(4): p. 1454-1463.
24. Sudipta Chatterjee, et al., Adsorption of a cationic dye, methylene blue, on to chitosan hydrogel beads generated by anionic surfactant gelation. Environmental Technology, 2011. 32(13): p. 1503-1514.
25. Sudipta Chatterjee, et al., Congo red adsorption from aqueous solutions by using chitosan hydrogel beads impregnated with nonionic or anionic surfactant. Bioresource Technology, 2009. 100(17): p. 3862-3868.
26. Haizhen Huang, Qiang Yuan, and X. Yang, Preparation and characterization of metal-chitosan nanocomposites. Colloids and Surfaces B: Biointerfaces, 2004. 39(1-2): p. 31-37.
27. Xuecai Tan, et al., An amperometric cholesterol biosensor based on multiwalled carbon nanotubes and organically modified sol-gel/chitosan hybrid composite film. Analytical Biochemistry, 2005. 337(1): p. 111-120.
28. Komathi, S., et al., Fabrication of a novel dual mode cholesterol biosensor using titanium dioxide nanowire bridged 3D graphene nanostacks. Biosensors and Bioelectronics, 2016. 84: p. 64-71.
29. Yao, T. and K. Takashima, Amperometric biosensor with a composite membrane of sol-gel derived enzyme film and electrochemically generated poly(1,2-diaminobenzene) film. Biosensors and Bioelectronics, 1998. 13(1): p. 67-73.
30. Özer, B.C., et al., Amperometric enzyme electrode for free cholesterol determination prepared with cholesterol oxidase immobilized in poly(vinylferrocenium) film. Enzyme and Microbial Technology, 2007. 40(2): p. 262-265.
31. Li, Y., et al., A nonenzymatic cholesterol sensor constructed by using porous tubular silver nanoparticles. Biosensors and Bioelectronics, 2010. 25(10): p. 2356-2360.
32. Huang, Q., et al., A dual enzymatic-biosensor for simultaneous determination of glucose and cholesterol in serum and peritoneal macrophages of diabetic mice: Evaluation of the diabetes-accelerated atherosclerosis risk. Analytica Chimica Acta, 2011. 707(1–2): p. 135-141.
33. Situmorang, M., P.W. Alexander, and D.B. Hibbert, Flow injection potentiometry for enzymatic assay of cholesterol with a tungsten electrode sensor. Talanta, 1999. 49(3): p. 639-649.
34. Pratima R. Solanki, et al., Nanostructured zinc oxide platform for cholesterol sensor. Applied Physics Letters, 2009. 94: p. 143901.

35. Ansari, A.A., et al., Electrochemical Cholesterol Sensor Based on Tin Oxide-Chitosan Nanobiocomposite Film. Electroanalysis, 2009. 21(8): p. 965-972.
36. Vidal, J.-C., et al., Amperometric cholesterol biosensors based on the electropolymerization of pyrrole and the electrocatalytic effect of Prussian-Blue layers helped with self-assembled monolayers. Talanta, 2004. 64(3): p. 655-664.
37. Giri, A.K., et al., Phase and composition selective superior cholesterol sensing performance of ZnO@ZnS nano-heterostructure and ZnS nanotubes. Sensors and Actuators B: Chemical, 2016. 229: p. 14-24.
38. Tapan Kumar Girin, et al., Modified chitosan hydrogels as drug delivery and tissue engineering systems: present status and applications. Acta Pharmaceutica Sinica B, 2012. 2(5): p. 439-449.
39. Kurt Ingar Draget, et al., Chitosan cross-linked with Mo(VI) polyoxyanions a new gelling system. Biomaterials, 1992. 13(9): p. 635-638.
40. R. Jayakumara, et al., Graft copolymerized chitosan-present status and applications. Carbohydrate Polymers, 2005. 62(2): p. 142-158.
41. X Qu, A Wirsén, and A.C. Albertsson, Novel pH-sensitive chitosan hydrogels swelling behavior andstates of water. Polymer. 41(12): p. 4589–4598.
42. Kozo Shinoda, Toshio Nakagawa, and B.-I. Tamamushi, The Formation of Micelles, in Colloidal Surfactants: Some Physicochemical Properties. 1963.
43. Digambara Patra, et al., Effect of curcumin on liposome: curcumin as a molecular probe for monitoring interaction of ionic liquids with 1,2-dipalmitoyl-sn-glycero-3-phosphocholine liposome. Photochemistry and Photobiology, 2012. 88(2): p. 317-327.
44. Elsy El Khoury and D. Patra, Ionic liquid expedites partition of curcumin into solid gel phase but discourages partition into liquid crystalline phase of 1,2-dimyristoyl-sn-glycero-3-phosphocholine liposomes. the Journal of Physical Chemistry B, 2013. 117(33): p. 9699-9708.
45. Elsy El Khoury, et al., Green synthesis of curcumin conjugated nanosilver for the applications in nucleic acid sensing and anti-bacterial activity. Colloids and Surfaces B: Biointerfaces, 2015. 127: p. 274-280.
46. Sujata M. Khopde, et al., Effect of solvent on the excited-state photophysical properties of curcumin. Photochemistry and Photobiology, 2000. 72(5): p. 625-631.
47. Colin F. Chigneli, et al., Spectral and Photochemical Proprieties of Curcumin. photochemistry and photobiology 1994. 59(3): p. 295-302.
48. Priyadarsini, K.I., Photophysics, photochemistry and photobiology of curcumin: Studies from organic solutions, bio-mimetics and living cells. Journal of Photochemistry and Photobiology C: Photochemistry Reviews, 2009. 10(2): p. 81-95.
49. Tsonko M. Kolev, et al., DFT and experimental studies of the structure and vibrational spectra of curcumin. International Journal of Quantum Chemistry, 2005. 102(6): p. 1069-1079.
50. Ying-Jan Wang, et al., Stability of curcumin in buffer solutions and characterization of its degradation products. Journal of Pharmaceutical and Biomedical Analysis, 1997. 15: p. 1867-1876.
51. Amrik Khurana and C.-T. Ho, High Performance Liquid Chromatographic Analysis of Curcuminoids and Their Photo-oxidative Decomposition

Compounds in Curcuma Longa L. Journal of Liquid Chromatography, 1988. 11(11): p. 2295-2304.
52. Yuan Zhao, et al., Enhanced stability of curcumin in colloidosomes stabilized by silica aggregates. LWT - Food Science and Technology, 2014. 58(2): p. 667-671.
53. Camila Sampaio Mangolim, et al., Curcumin-beta-cyclodextrin inclusion complex: stability, solubility, characterisation by FT-IR, FT-Raman, X-ray diffraction and photoacoustic spectroscopy, and food application. Food Chemistry, 2014. 153: p. 361-370.
54. N. Sanoj Rejinolda, et al., Curcumin-loaded biocompatible thermoresponsive polymeric nanoparticles for cancer drug delivery. Journal of Colloid and Interface Science, 2011. 360(1): p. 39-51.
55. Alfeu Zanotto-Filho, et al., Curcumin-loaded lipid-core nanocapsules as a strategy to improve pharmacological efficacy of curcumin in glioma treatment. European Journal of Pharmaceutics and Biopharmaceutics, 2013. 83(2): p. 156-167.
56. Lan Li, Fadi S. Braiteh, and R. Kurzrock, Liposome-encapsulated curcumin: in vitro and in vivo effects on proliferation, apoptosis, signaling, and angiogenesis. Cancer, 2005. 104(6): p. 1322-1331.
57. Banerjee, S. and A.R. Chakravarty, Metal complexes of curcumin for cellular imaging, targeting, and photoinduced anticancer activity. Acc Chem Res, 2015. 48(7): p. 2075-83.
58. Michael Pröhl, et al., Metal complexes of curcumin and curcumin derivatives for molecular imaging and anticancer therapy. Coordination Chemistry Reviews, 2016. 307: p. 32-41.
59. K. Varaprasad, et al., Synthesis and characterization of hydrogel-silver nanoparticle-curcumin composites for wound dressing and antibacterial application. Journal of Applied Polymer Science, 2011. 121(2): p. 784-796.
60. Priyadarsini, K.I., The chemistry of curcumin: from extraction to therapeutic agent. Molecules, 2014. 19(12): p. 20091-20112.
61. Supat Buddee, et al., Curcumin-sensitized TiO2 for enhanced photodegradation of dyes under visible light. Journal of Nanoparticle Research, 2014. 16(4).
62. K. Vignesh, et al., Photocatalytic performance of Ag doped SnO2 nanoparticles modified with curcumin. Solid State Sciences, 2013. 21: p. 91-99.
63. James V. Crivello and U. Bulut, Curcumin: A naturally occurring long-wavelength photosensitizer for diaryliodonium salts. Journal of Polymer Science Part A: Polymer Chemistry, 2005. 43(21): p. 5217-5231.
64. S. Bettini, et al., Drastic nickel ion removal from aqueous solution by curcumin-capped Ag nanoparticles. Nanoscale, 2014. 6(17): p. 10113-10117.
65. Amornrat Saithongdee, Narong Praphairaksit, and A. Imyim, Electrospun curcumin-loaded zein membrane for iron(III) ions sensing. Sensors and Actuators B: Chemical, 2014. 202: p. 935-940.
66. Nahid Pourreza and H. Golmohammadi, Application of curcumin nanoparticles in a lab-on-paper device as a simple and green pH probe. Talanta, 2015. 131: p. 136-141.
67. Mária Pávai, Judith Mihály, and A. Paszternák, pH and CO2 Sensing by Curcumin-Coloured Cellophane Test Strip. Food Analytical Methods, 2015. 8(9): p. 2243-2249.

68. Bernard Valeur and M.r.N. Berberan-Santos, A Brief History of Fluorescence and Phosphorescence before the Emergence of Quantum Theory. Journal of Chemical Education, 2011. 88(6): p. 731-738.
69. Lakowicz, J.R., Principles of Fluorescence Spectroscopy, Springer, Editor. 2006.
70. Benoit Magny, I.I., Raoul Zana, Roland Audebert, Mixed micelles formed by cationic surfactants and anionic hydrophobically modified polyelectrolytes. Langmuir, 1994. 10(9): p. 3180-3187.
71. Polymer—surfactant interaction part II Polymer and surfactant of opposite charge.
72. Digambara Patra, C.B., Unique role of ionic liquid [bmin][BF4] during curcumin-surfactant association and micellization of cationic, anionic and non-ionic surfactant solutions. Spectrochimica Acta Part A: Molecular and Biomolecular Spectroscopy, 2011. 79(5): p. 1823-1828.
73. Digambara Patra, Diana Ahmadieh, and R. Aridi, Study on interaction of bile salts with curcumin and curcumin embedded in dipalmitoyl-sn-glycero-3-phosphocholine liposome. Colloids and Surfaces B: Biointerfaces, 2013. 110: p. 296-304.
74. Mai Mouslmani, Kamal H. Bouhadir, and D. Patra, Poly (9-(2-diallylaminoethyl)adenine HCl-co-sulfur dioxide) deposited on silica nanoparticles constructs hierarchically ordered nanocapsules: curcumin conjugated nanocapsules as a novel strategy to amplify guanine selectivity among nucleobases. Biosensors and Bioelectronics, 2015. 68: p. 181-188.
75. Digambara Patra, R.A., Kamal Bouhadir, Fluorometric sensing of DNA using curcumin encapsulated in nanoparticle-assembled microcapsules prepared from poly(diallylammonium chloride-co-sulfur dioxide). Microchimica Acta, 2012. 180(1-2): p. 59-64.
76. Rasha N. Moussawi and D. Patra, Synthesis of Au nanorods through prereduction with curcumin: Preferential enhancement of Au nanorod formation prepared from CTAB-capped over citrate-capped Au seeds. The Journal of Physical Chemistry C, 2015. 119(33): p. 19458-19468.
77. Paul C. Hiemenz, R.R., Principles of colloid and surface chemistry.
78. Milton J. Rosen, J.H.M., Lesley Davenport, Aberrant aggregation behavior in cationic gemini surfactants investigated by surface tension, interfacial tension, and fluorescence methods. Langmuir, 1999. 15(21): p. 7340-7346.
79. K. Kalyanasundaram, J.K.T., Environmental effects on vibronic band intensities in pyrene monomer fluorescence and their application in studies of micellar systems. Journal of the American Chemical Society 1977. 99(7): p. 2039-2044.
80. Andreas Mohr, P.T., Hans-Gert Korth, Reiner Sustmann, Roland Boese, Dieter Bläser, Heinz Rehage, A new pyrene-based fluorescent probe for the determination of critical micelle concentrations. The Journal of Physical Chemistry B, 2007. 111(45): p. 12985-12992.
81. Robin Humphry-Baker, M.G., Yoshikiyo Moroi, Pyrene fluorescence at air/sodium dodecyl sulfate solution interface. Langmuir, 2006. 22(26): p. 11205-11207.
82. P. C. Shanks, E.I.F., Estimation of micellization parameters of aqueous sodium dodecyl sulfate from conductivity data. the journal of physical Chemistry 1992. 96(4): p. 1794-1805.

83. J. Sujatha, A.K.M., Phase transitions in phospholipid vesicles excited state prototropism of 1-naphthol as a novel probe concept. Langmuir, 1998. 14(9): p. 2256-2262.
84. Masanobu Mizusaki, Y.M., Paul L. Dublin, Interaction of pyrene-labeled hydrophobically modified polyelectrolytes with oppositely charged mixed micelles studied by fluorescence quenching. the journal of physical Chemistry B, 1998. 102(11): p. 1908-1915.
85. Yotaro Morishima, M.M., Katsunori Yoshidab, Paul L. Dubin, Interactions of micelles with fluorescence-labeled polyelectrolytes. Colloids and Surfaces A: Physicochemical and Engineering Aspects, 1999. 147(1-2): p. 149-159.
86. D.K. Palit, A.V.S., J.P. Mittal, Picosecond studies on the electron transfer from pyrene and perylene excited singlet states to N-hexadecyl pyridinium chloride. Chemical Physics Letters, 1997. 269(3-4): p. 286-292.
87. Jeffrey Barry, M.F., Jeffrey R. Brender, Pieter E. S. Smith, Dong-Kuk Lee, Ayyalusamy Ramamoorthy Determining the effects of lipophilic drugs on membrane structure by solid-state NMR spectroscopy: the case of the antioxidant curcumin. Journal of the American Chemical Society, 2009. 131(12): p. 4490-4498.
88. Angel Pérez-Lara, A.A., Francisco J. Aranda, Ana de Godos, Alejandro Torrecillas, Senena Corbalán-García, Juan C. Gómez-Fernández, Curcumin disorders 1,2-Dipalmitoyl-sn-glycero-3-phosphocholine membranes and favors the formation of nonlamellar structures by 1,2-Dielaidoyl-sn-glycero-3-phosphoethanolamine. the Journal of Physical Chemistry B, 2010. 114(30): p. 9778-9786.
89. Kazimiera A. Wilk, U.L., Katarzyna Zielińska, Andrzej Olszowski, Fluorescence probe studies upon microenvironment characteristics and aggregation properties of gemini sugar surfactants in an aquatic environment. Journal of Photochemistry and Photobiology A: Chemistry, 2011. 219(2-3): p. 204-210.
90. Nicholas J. Turro, A.Y., Luminescent probes for detergent solutions. A simple procedure for determination of the mean aggregation number of micelles. Journal of the American Chemical Society, 1978. 100(18): p. 5951-5952.
91. Jan Kevelam, J.B.F.N.E., Aggregation numbers of hydrophobic microdomains formed from Poly(dimethyldiallylammonium-co-methyl-n-dodecyldiallylammonium) salts in aqueous solutions. Journal of Colloid and Interface Science, 1996. 178(1): p. 87-92.
92. Kazunari Akiyoshi, et al., Self-aggregates of hydrophobized polysaccharides in water. Formation and characteristics of nanoparticles. Macromolecules, 1993. 26(12): p. 3062-3068.
93. J. Sunamoto, K.A., S. Deguchi, Y. Kato, I. Taniguchii, Y. Sasaki, K. Kuroda, Hydrogel nanoparticles formed by self-aggregation of hydrophobized polysaccharides. Abstracts of Papers of the American Chemical Society, 1998. 216: p. 831.
94. Alexander V. Kabanov, S.V.V., Nanogels as pharmaceutical carriers: finite networks of infinite capabilities. Angewandte Chemie, 2009. 48(30): p. 5418-5429.

95. Nobuyuki Morimoto, S.-i.M.N., Naomi Miyazawa, Kazunari Akiyoshi, Nanogel engineered designs for polymeric drug delivery, in Polymeric Drug Delivery II. 2006, American Chemical Society. p. 88-101.
96. Kuen Yong Lee, W.H.J., Ick Chan Kwon, Yong-Hee Kim, Seo Young Jeong, Structural determination and interiorpolarity of self-aggregates prepared from deoxycholic acid-modified chitosan in water. Macromolecules 19998. 31(2): p. 378-383.
97. Marieta Nichifor, A.L., Adrian Carpov, Eurico Melo, Aggregation in water of dextran hydrophobically modified with bile acids. Macromolecules, 1999. 32(21): p. 7078-7085.
98. G. Began, E.S., K. Udaya Sankar, A. G. Appu Rao, Interaction of curcumin with phosphatidylcholine: A spectrofluorometric study. Journal of Agricultural and Food Chemistry, 1999. 47(12): p. 4992-4997.
99. Atanu Barik, B.M., Amit Kunwar, K. Indira Priyadarsini, Interaction of curcumin with human serum albumin: Thermodynamic properties, fluorescence energy transfer and denaturation effects. Chemical Physics Letters, 2007. 436(1-3): p. 239-243.
100. Germershaus, O., et al., Gene delivery using chitosan, trimethyl chitosan or polyethylenglycol-graft-trimethyl chitosan block copolymers: establishment of structure-activity relationships in vitro. J Control Release, 2008. 125(2): p. 145-54.
101. Amitabha Chattopadhyay, K.G.H., Dependence of critical micelle concentration of a zwitterionic detergent on ionic strength: implications in receptor solubilization. FEBS Letters, 1996. 391(1-2): p. 199-202.
102. Zhijian Huang and R.P. Haugland, Partition coefficients of fluorescent probes with phospholipid membranes. Biochemical and Biophysical Research Communications, 1991. 181(1): p. 166-171.
103. Smart Polymers and their Applications. Woodhead Publishing in Materials. 2014: Woodhead Publishing.
104. Shtykov, S.N. and T.Y. Rusanova, Nanomaterials and nanotechnologies in chemical and biochemical sensors: Capabilities and applications. Russian Journal of General Chemistry, 2008. 78(12): p. 2521-2531.
105. Sassolas, A., B.D. Leca-Bouvier, and L.J. Blum, DNA Biosensors and Microarrays. Chemical Reviews, 2008. 108(1): p. 109-139.
106. Jung Kwon Oha, Do Ik Lee , and J.M. Park, Biopolymer-based microgels/nanogels for drug delivery applications. Progress in Polymer Science, 2009. 34(12): p. 1261-1282.
107. Brian H. Morrow, Gregory F. Payne, and J. Shen, pH-Responsive self-assembly of polysaccharide through a rugged energy landscape. Journal of the American Chemical Society 2015. 137(40): p. 13024-13030.
108. Wipa Suginta, Panida Khunkaewla, and A. Schulte, Electrochemical biosensor applications of polysaccharides chitin and chitosan. Chemical Reviews, 2013. 113(7): p. 5458-5479.
109. Michael D. Buschmann, et al., Chitosans for delivery of nucleic acids. Advanced Drug Delivery Reviews, 2013. 65(9): p. 1234-1270.
110. M. N. V. Ravi Kumar, et al., Chitosan chemistry and pharmaceutical perspectives. Chemical Reviews, 2004. 104(12): p. 6017-6084.

111. Eugene Khor and L.Y. Lim, Implantable applications of chitin and chitosan. Biomaterials, 2003. 24(13): p. 2339-2349.
112. Eunkyoung Kim, et al., Chitosan to connect biology to electronics: Fabricating the bio-device interface and communicating across this interface. Polymers, 2015. 7(1): p. 1-46.
113. Tao Jiang, M.D., Roshan James, Lakshmi S. Nair, Cato T. Laurencin, Micro- and nanofabrication of chitosan structures for regenerative engineering. Acta Biomaterialia, 2014. 10(4): p. 1632-1645.
114. Perry F. Churchill and T. Kimura, Topological studies of cytochromes $P450_{scc}$ and $P450_{11\beta}$ in bovine adrenocortical inner mitochondrial membranes. Effects of controlled tryptic digestion. . the Journal of Biological Chemistry 1979. 254(20): p. 10443-10448.
115. Sadava, D.E., et al., Life: The Science of Biology. Vol. 1. 2009: Macmillan.
116. Klaus Podar and K.C. Anderson, Caveolin-1 as a potential new therapeutic target in multiple myeloma. Cancer Letters, 2006. 233(1): p. 10-15.
117. Joseph L. Goldstein and M.S. Brown, Regulation of the mevalonate pathway. Nature, 1990. 343(6257): p. 425-430.
118. Ikonen, E., Cellular cholesterol trafficking and compartmentalization. Nature Reviews Molecular Cell Biology, 2008. 9(2): p. 125-38.
119. George Yuan, Jian Wang, and R.A. Hegele, Heterozygous familial hypercholesterolemia: an underrecognized cause of early cardiovascular disease. Canadian Medical Association Journal, 2006. 174(8): p. 1124-1129.
120. Sjogren, M. and K. Blennow, The link between cholesterol and Alzheimer's disease. The World Journal of Biological Psychiatry, 2005. 6(2): p. 85-97.
121. Kritchevsky, S.B., Serum Cholesterol and Cancer Risk: An Epidemiologic Perspective. Annual Review of Nutrition, 1992. 12: p. 391-416.
122. Michael J. Pencina, et al., Application of New Cholesterol Guidelines to a Population-Based Sample. New England Journal of Medicine, 2014. 370(15): p. 1422-1431.
123. David Saraiva, et al., Selection of the derivatization reagent—The case of human blood cholesterol, its precursors and phytosterols GC–MS analyses. Journal of Chromatography B, 2011. 879(32): p. 3806-3811.
124. Anjan Kumar Basu, et al., Development of cholesterol biosensor based on immobilized cholesterol esterase and cholesterol oxidase on oxygen electrode for the determination of total cholesterol in food samples. Bioelectrochemistry, 2007. 70(2): p. 375-379.
125. Marco Mascini, Mauro Tomassetti, and M. Iannello, Determination of free and total cholesterolin human bile samples using an enzyme electrode. Clinica Chimica Acta, 1983. 132: p. 7-15.
126. Shaojun Dong, Qing Deng, and G. Cheng, Cholesterol sensor based on electrodeposition of catalytic palladium particles. Analytica Chimica Acta, 1993. 279: p. 235-240.
127. Fadime Yıldırımoğlu, et al., Preparation of a polypyrrole-polyvinylsulphonate composite film biosensor for determination of cholesterol based on entrapment of cholesterol oxidase. Sensors (Basel), 2009. 9(8): p. 6435-6445.
128. Lin Xu, et al., Electrochemical sensor based on a silver nanowires modified electrode for the determination of cholesterol. Analytical Methods, 2015. 7(13): p. 5649-5653.

129. Zhenjiang Li, et al., Direct electrochemistry of cholesterol oxidase immobilized on chitosan–graphene and cholesterol sensing. Sensors and Actuators B: Chemical, 2015. 208: p. 505-511.
130. Lian Zhu, et al., Direct electrochemistry of cholesterol oxidase immobilized on gold nanoparticles-decorated multiwalled carbon nanotubes and cholesterol sensing. Talanta, 2013. 106: p. 192-199.
131. Revanasiddappa Manjunatha, et al., Direct electrochemistry of cholesterol oxidase on MWCNTs. Journal of Electroanalytical Chemistry, 2011. 651(1): p. 24-29.
132. Nan Li, et al., Ultrasensitive Profiling of Metabolites Using Tyramine-Functionalized Graphene Quantum Dots. ACS Nano, 2016. 10(3): p. 3622-3629.
133. Ki-Eun Kim, Tae Geun Kim, and Y.-M. Sung, Fluorescent cholesterol sensing using enzyme-modified CdSe/ZnS quantum dots. Journal of Nanoparticle Research, 2012. 14(10).
134. Yang Cheng, et al., An imprinted fluorescent chemosensor prepared using dansyl-modified β-cyclodextrin as the functional monomer for sensing of cholesterol with tailor-made selectivity. Sensors and Actuators B: Chemical, 2014. 193: p. 838-843.
135. Marie E. Egan, et al., Curcumin, a major constituent of turmeric, corrects cystic fibrosis defects. Science 2004. 304: p. 600-602.
136. Melessa Salem, Sohrab Rohani, and E.R. Gillies, Curcumin, a promising anti-cancer therapeutic: a review of its chemical properties, bioactivity and approaches to cancer cell delivery. Royal Society of Chemistry Advances, 2014. 4(21): p. 10815-10829.
137. Fusheng Yang, et al., Curcumin inhibits formation of amyloid β oligomers and fibrils, binds plaques, and reduces amyloid in vivo. Journal of Biological Chemistry, 2005. 280(7): p. 5892-5901.
138. Avi Khafif, et al., Quantitation of chemopreventive synergism between (-)-epigallocatechin-3-gallate and curcumin in normal, premalignant and malignant human oral epithelial cells. Carcinogenesis 1998. 19(3): p. 419-424.
139. Alwi, I., et al., The effect of curcumin on lipid level in patients with acute coronary syndrome. Acta Med Indonesiana, 2008. 40(4): p. 201-210.
140. Chebl, M., et al., Two Modes of Associations of Curcumin with Pre- and Nanoaggregated Chitosan Oligosaccharide Lactate: Ionic Strength and Hydrophobic Bile Salt Modulate Partition of Drug and Self-Assembly Process. The Journal of Physical Chemistry C, 2016. 120(20): p. 11210-11224.
141. Mai Mouslmani and D. Patra, Revoking excited state intra-molecular hydrogen transfer by size dependent tailor-made hierarchically ordered nanocapsules. RSC Advances, 2014. 4(16): p. 8317.
142. Digambara Patra and F. Sleem, A new method for pH triggered curcumin release by applying poly(l-lysine) mediated nanoparticle-congregation. Analytica Chimica Acta, 2013. 795: p. 60-68.
143. Patra, D., A.J. Amali, and R.K. Rana, Preparation and photophysics of HPTS-based nanoparticle-assembled microcapsules. Journal of Materials Chemistry, 2009. 19(23): p. 4017-4021.
144. Lai, S.M., et al., The Properties and Preparation of Chitosan/Silica Hybrids Using Sol-Gel Process. Polymer-Plastics Technology and Engineering, 2006. 45(9): p. 997-1003.

145. Abdelwahed, W., et al., Freeze-drying of nanoparticles: Formulation, process and storage considerations☆. Advanced Drug Delivery Reviews, 2006. 58(15): p. 1688-1713.
146. Shaikh, J., et al., Nanoparticle encapsulation improves oral bioavailability of curcumin by at least 9-fold when compared to curcumin administered with piperine as absorption enhancer. European Journal of Pharmaceutical Sciences, 2009. 37(3-4): p. 223-230.
147. Ferenc Zsila, Zsolt Bikádi, and M. Simonyi, Molecular basis of the Cotton effects induced by the binding of curcumin to human serum albumin. Tetrahedron: Asymmetry, 2003. 14(16): p. 2433-2444.
148. Ling Kong, K. Indira Priyadarsini, and H.-Y. Zhang, A theoretical investigation on intramolecular hydrogen-atom transfer in curcumin. Journal of Molecular Structure: THEOCHEM, 2004. 684(1–3): p. 111-116.
149. Carlos R. Baiz and B.D. Dunietz, Theoretical Studies of Conjugation Effects on Excited State Intramolecular Hydrogen-Atom Transfer Reactions in Model Systems. The Journal of Physical Chemistry A, 2007. 111(40): p. 10139-10143.
150. Galasso, V., et al., Spectroscopic and Theoretical Study of the Electronic Structure of Curcumin and Related Fragment Molecules. The Journal of Physical Chemistry A, 2008. 112(11): p. 2331-2338.
151. Liang Shen, Hong-Yu Zhang , and H.-F. Ji, Successful Application of TD-DFT in Transient Absorption Spectra Assignment. Organic Letters, 2005. 7(2): p. 243-246.
152. Liang Shen and H.-F. Ji, Theoretical study on physicochemical properties of curcumin. Spectrochimica Acta Part A: Molecular and Biomolecular Spectroscopy, 2007. 67(3–4): p. 619-623.
153. Kim, S.-H., et al., The photo- and electrophysical properties of curcumin in aqueous solution. Spectrochimica Acta Part A: Molecular and Biomolecular Spectroscopy, 2010. 76(3–4): p. 384-387.
154. Zhao, X.-Z., et al., Interaction of curcumin with Zn(II) and Cu(II) ions based on experiment and theoretical calculation. Journal of Molecular Structure, 2010. 984(1–3): p. 316-325.
155. Qu, R., et al., Preparation and metal-binding behaviour of chitosan functionalized by ester- and amino-terminated hyperbranched polyamidoamine polymers. Carbohydrate Research, 2008. 343(2): p. 267-273.
156. Heng-Chia Chang and J.-a.A. Ho, Gold Nanocluster-Assisted Fluorescent Detection for Hydrogen Peroxide and Cholesterol Based on the Inner Filter Effect of Gold Nanoparticles. Analytical Chemistry, 2015. 87(20): p. 10362-10367.
157. Drake M. Amundson and M. Zhou, Fluorometric method for the enzymatic determination of cholesterol. Journal of Biochemical and Biophysical Methods, 1999. 38(1): p. 43-52.
158. Ning Zhang, et al., A novel assembly of Au NPs-β-CDs-FL for the fluorescent probing of cholesterol and its application in blood serum. Analyst, 2008. 133(9): p. 1176-1181.
159. Ding, Y., et al., An upconversion nanocomposite for fluorescence resonance energy transfer based cholesterol-sensing in human serum. Nanoscale, 2014. 6(24): p. 14792-8.

160. Connors, K.A., Binding constants: the measurement of molecular complex stability. 1987, New York: John Wiley & Sons.
161. Paradkar, M.M. and J. Irudayaraj, Determination of cholesterol in dairy products using infrared techniques: 1. FTIR spectroscopy. International Journal of Dairy Technology, 2002. 55(3): p. 127-132.